Bioorganic Chemistry 92 (2019) 103212

Contents lists available at ScienceDirect

Bioorganic Chemistry

journal homepage: www.elsevier.com/locate/bioorg

# Coumarin tethered cyclic imides as efficacious glucose uptake agents and investigation of hit candidate to probe its binding mechanism with human serum albumin

Dinesh S. Reddy[a], Manasa Kongot[a], Vishal Singh[b], Neha Maurya[c], Rajan Patel[c], Nitin Kumar Singhal[b], Fernando Avecilla[d], Amit Kumar[a,*]

[a] Centre for Nano and Material Sciences, Jain University, Jain Global Campus, Jakkasandra Post, Bangalore 562112, India
[b] National Agri Food Biotechnology Institute, Mohali 140306, India
[c] Biophysical Chemistry Laboratory, Centre for Interdisciplinary Research in Basic Sciences, Jamia Millia Islamia (A Central University), New Delhi 110025, India
[d] Grupo Xenomar, Centro de Investigacións Científicas Avanzadas (CICA), Departamento de Química, Facultade de Ciencias, Universidade da Coruña, Campus de A Coruña, 15071 A Coruña, Spain

ARTICLE INFO

*Keywords:*
Coumarins
Cyclic imides
Glucose uptake
Human serum albumin (HSA)
Solution stability studies

ABSTRACT

A series of novel coumarin-cyclic imide conjugates (**1a–1j**) were designed and synthesized to evaluate their glucose uptake activity by insulin resistant liver hepatocyte carcinoma (HepG2) cells through 2-NBDG uptake assay. Compounds (**1a–1j**) were characterised using various analytical methods such as $^{1}$H NMR, $^{13}$C NMR, IR, GC–MS, elemental and single-crystal X-ray diffraction techniques. Compounds (**1a–1j**) exhibited 85.21 – 65.80% of glucose uptake and showed low level of cytotoxicity towards human embryonic kidney cells (HEK-293) indicating good selectivity and safety profile. Compound **1f** was identified as a hit candidate exhibiting 85.21% of glucose uptake which was comparable with standard antidiabetic drug Metformin (93.25% glucose uptake). Solution stability study under physiological pH conditions ≈ (3.4 – 8.7), indicates that compound **1f** is sufficiently stable at varied pH conditions and thereby compatible with bio-physiological environments. Interaction of **1f** with human serum albumin (HSA) were also studied which quantifies that compound **1f** binds with HSA efficiently through facile binding reaction in solution. Fluorescence, UV–vis spectrophotometry and molecular modeling methodologies were employed for studying the interaction mechanism of compound **1f** with protein.

## 1. Introduction

Diabetes affects a large section of the world population with an estimation of 1.6 million deaths worldwide in 2015 alone. As per World Health Organization (WHO), the number of diabetic patients have increased from 0.18 billion in 1980 to 0.42 billion in 2014, indicating its alarming prevalence in the coming decades [1]. Among the different categories of diabetes, type-2 diabetes affects the larger population, accounting for 90% of all diabetic cases. This condition involves the loss of insulin sensitivity by the body cells, thereby causing hyperglycemia [2].

Today most of the antidiabetic drugs generally include insulin secreting agents such as Sulfonylureas, Glinides, Thiazolidinediones and Biguanides which perform *via* the mechanism of α-glucosidase inhibition [3]. Recently, dipeptidyl peptidase IV (DPP-IV) inhibitors which work by inhibiting incretin catabolism and thus increasing insulin secretion, have also emerged as promising antidiabetic agents to treat type-2 diabetes [4]. To name a few, Sitagliptin, Saxagliptin, Vidagliptin, Linagliptin, Omarigliptin and Alogliptin are among the different classes of DPP-IV inhibitors [3–5]. Although DPP-IV inhibitors are effective in diabetic treatment, majority of such drugs have certain side effects such as weight gain, edema, fractures, lactic acidosis, gastrointestinal intolerance, hypoglycaemia and cardiovascular diseases [3,6–8]. Thereby, it is a challenging task for the researchers to develop an effective and safe anti-diabetic drugs in order to minimize the diabetic complications from the patient's body.

Coumarin scaffolds are well established structural motifs found mainly in plants and in some microorganisms [9]. They have found to exhibit a broad range of bioactivities and thereby, have been evolved as favourable lead targets for medicinal uses [9,10]. Further, coumarin has a unique character which allows its derivatives to interact easily with various enzymes through weak bond interactions and thereby have

* Corresponding author.
*E-mail address:* amit.kumar@jainuniversity.ac.in (A. Kumar).

https://doi.org/10.1016/j.bioorg.2019.103212
Received 7 June 2019; Received in revised form 6 August 2019; Accepted 20 August 2019
Available online 21 August 2019
0045-2068/ 

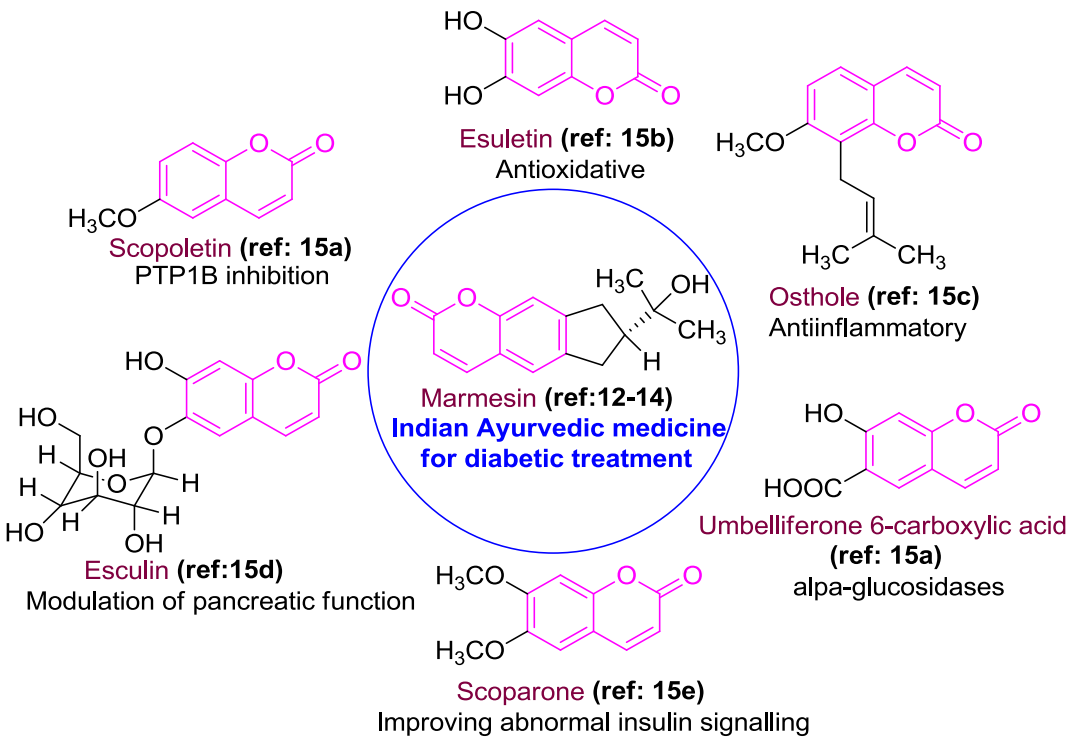


**Fig. 1.** Marmesin, an Indian Ayurvedic medicine used for diabetic treatment and structures of some coumarin analogs exhibiting anti-diabetic affects by various mechanisms.

greater scope as medicinal drugs [11]. Among the various biological activities, antidiabetic activity of coumarin is well known from ancient times, e.g. Marmesin, a coumarin derivative has been used against diabetes in Indian Ayurvedic medicine [12–14]. It is known that coumarins (Fig. 1) exhibit their antidiabetic effects by various mechanisms [15] such as antioxidative [15b], antiinflammatory action [15c], modulation of pancreatic function [15d], improvement of abnormal insulin signalling [15e], α-glucosidase inhibition [15a,15f], and PTP1B inhibition [15a]. However, despite its unique and widespread pharmacological properties, extensive efforts were not made in designing coumarin-based antidiabetic drugs. This prompted researchers to exploit antidiabetic potential of this class of compounds and thus synthetic coumarin analogs have been recently developed and reported to display significant antidiabetic effects [16–18].

Cyclic imides are another important class of compounds with unique pharmacokineticproperties [19] and are known to possess diverse medicinal activities such as antibacterial [20], antifungal [21], antitumor [22], antitubercular [23] and analgesic activities [20]. Recently, 4,4-dimethylpiperidine-2,6-dione derived compounds were explored as effective antihypertensive agents revealing the therapeutic potential of cyclic imide scaffold [24]. In particular, cyclic imides can also be found in several antidiabetic drugs such as Trelagliptin [25], Alogliptin [26] and Linagliptin [27] which are known for treating type-2 diabetes. Another favourable cyclic imide inhibitor Fidarestat [28] is under clinical trials and has shown to inhibit the functional developments of diabetic neuropathy [29] and also halt the growth in sorbitol pathway flux in diabetic patients [30]. In some case, compound having cyclic imide ring have shown distinct antidiabetic activity than the standard drug Glibenclamide [31]. Structures of some antidiabetic drugs (Trelagliptin, Alogliptin, Linagliptin) and agent (Fidarestat) with cyclic imide ring are represented in Fig. 2.

Considering all the aforementioned pharmacological significance of cyclic imides particularly in diabetic treatment enthralled our curiosity in exploring these versatile motifs as conjugates with bio-active coumarin analogs, so that the synergetic effect of such combination may help in enhancing the overall activity of the compound. Apart from designing the desired compounds, it was also essential to see that the compounds fall well within the Lipinski rule of five (RO5) [32]. Reports have suggested that candidate drugs that conform to the RO5 tend to have lower attrition rates during clinical trials and hence have an increased chance of reaching the market [32,33]. Hence, keeping these factors in view the architecture of the compounds was designed (Fig. 3).

In the present study, we have designed, synthesized and characterized ten structural analogues of coumarin-cyclic imide conjugates. All the compounds were investigated for *in-vitro* glucose uptake activity potency and their safety profile on healthy cells. The solution state stability behavior over a wide range of pH conditions were studied to predict their nature under physiological environment. The most active compound was further studied for its interaction with human serum albumin protein (HSA).

## 2. Results and discussion

### 2.1. Chemistry

In order to synthesize the requisite coumarin-cyclic imide conjugates (**1a–1j**), $S_N2$ substitution reaction was employed (Scheme 1). The starting material, 4-bromomethyl coumarin derivatives [34] **(a–j)** were synthesized through Pechmann cyclization of phenols **(iii)** with ethyl 4-bromoacetoacetate **(ii)** using $H_2SO_4$ as cyclizing agent. The obtained 4-bromomethyl coumarin derivatives **(a–j)** on treating with 4,4-dimethylpiperidine-2,6-dione **(iv)** in presence of anhydrous $K_2CO_3$ afforded coumarin cyclic-imide derivatives (**1a-1j**) with 73–83% yields. The structures of the new compounds were confirmed by $^1$H NMR, $^{13}$C NMR, mass, IR and elemental analysis. Further, through single crystal X-ray diffraction, structures of compounds **1a-1f, 1h** and **1i** were elucidated.

In the case of compound **1a** (R = 6-$CH_3$), in the $^1$H NMR spectrum, a sharp singlet was observed in the up-field region at $\delta$ 1.14 ppm which corresponds to the di-methyl protons of the glutarimide ring. The two methylene protons at ortho position of glutarimide ring were observed as singlet at $\delta$ 2.62 ppm. The methyl proton at C-6 position of the

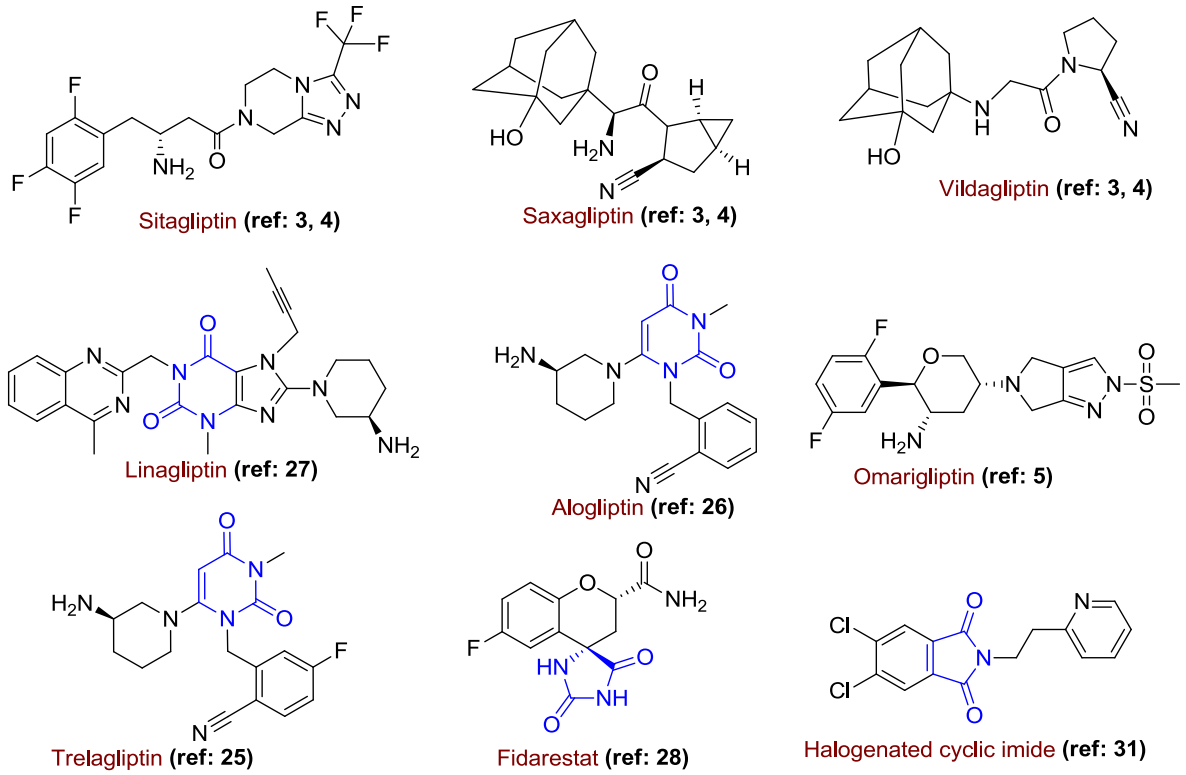


**Fig. 2.** Structures of some antidiabetic drugs and agents. Most of the compounds contain cyclic imide ring (drawn in blue).

coumarin was observed as singlet at $\delta$ 2.39 ppm. The methylene proton ($-CH_2$) linking the coumarin with glutarimide ring was observed as singlet at $\delta$ 5.10 ppm. Two singlets were observed at $\delta$ 5.90 ppm and $\delta$ 7.42 ppm corresponding to the $C_2$-H and $C_5$-H of the coumarin moiety respectively. The remaining aromatic protons of the coumarin unit were observed in the range $\delta$ 7.20–7.34 ppm. $^{13}C$ NMR data also support the structure of **1a**, wherein the two carbonyl carbons of the glutarimide ring were observed at $\delta$ 166.75 ppm and the carbonyl carbon of the coumarin moiety was observed at $\delta$ 155.85 ppm. The two methyl carbons of the glutarimide ring were observed at $\delta$ 23.12 and $\delta$ 23.22 ppm respectively. The methylene carbon of the glutarimide ring was observed at $\delta$ 34.21 ppm, whereas the methylene carbon connecting coumarin to glutarimide ring was observed at $\delta$ 41.38 ppm. The carbon at $C_2$ position of the coumarin ring was observed at $\delta$ 106.82 ppm. The remaining aromatic carbons showed signals in the range $\delta$ 112.25–146.91 ppm and are in good agreement with the predicted values. The molecular ion peak at 313 $[M]^+$ also confirmed the structure of **1a**. Spectral data of all other compounds are also in good agreement with their assigned structures (See Supporting Information page no. **S2–S11**).

### 2.2. X-ray crystal structure determination

Bruker Kappa Apex CCD diffractometer were used to collect 3-D X-ray crystal information for compounds **1a-1f, 1h** and **1i** by using the $\phi$-$\omega$ scan method. Reflections were measured using a hemisphere of data, each covering 0.3° in $\omega$ and collected from frames. A total of 53,993 for **1a**, 29,522 for **1b**, 37,632 for **1c**, 30,537 for **1d**, 34,083 for **1e**, 31,606 for **1f**, 35,538 for **1 h** and 144,652 for **1i**, reflections measured were corrected for absorption by multi-scan methods and for Lorentz and polarization effects by symmetry equivalent reflections. Of the total, 3197 for **1a**, 2856 for **1b**, 2970 for **1c**, 2878 for **1d**, 3042 for **1e**, 2962 for **1f**, 3008 for **1h** and 12,051 for **1i**, independent reflections surpassed the significance level ($|F|/\sigma|F|$) > 4.0. Upon data collection, a multi-scan absorption correction (SADABS) [35] was induced in each and every scan, and the structure was solved and refined by direct methods and full matrix least-squares on $F^2$ data respectively using SHELX program suite [36]. All hydrogen atoms were included in calculated positions and refined through the riding mode for all structures, except for **1a**, which was located in a different Fourier map and left to refine freely. Refinements were carried by allocation for thermal anisotropy of non-hydrogen atoms. ORTEP diagrams for compounds **1a-1f, 1h** and **1i** are shown in Fig. 4. Further details of the crystal structure refinement for the compounds are given in Table 1. Selected bond distances and angles are given in Supporting Information (see page no. **S25**).

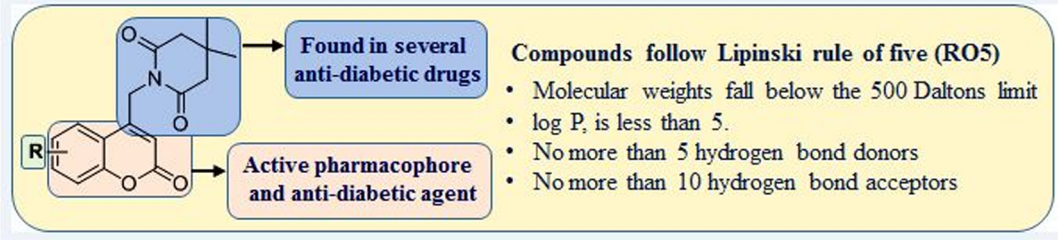


**Fig. 3.** Designed structural analogs which follow the Lipinski rule of five.

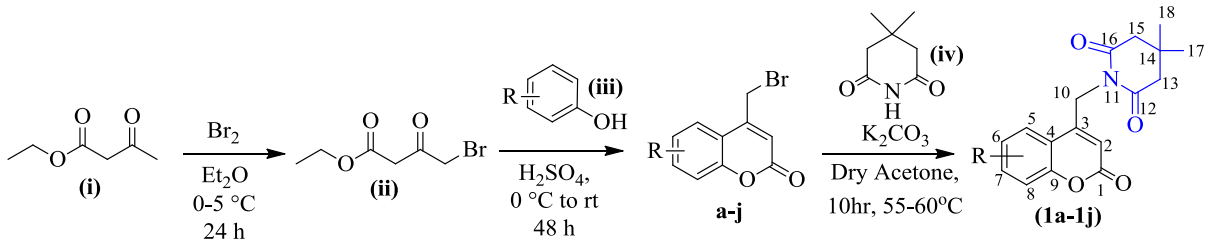


R = **(1a)** 6-Me, **(1b)** 7-Me, **(1c)** 6-Cl, **(1d)** 7-Cl, **(1e)** 5,7-diMe, **(1f)** 7,8-diMe, **(1g)** 7-OMe, **(1h)** 6-Br, **(1i)** 5,6-Benzo, **(1j)** 7,8-Benzo.

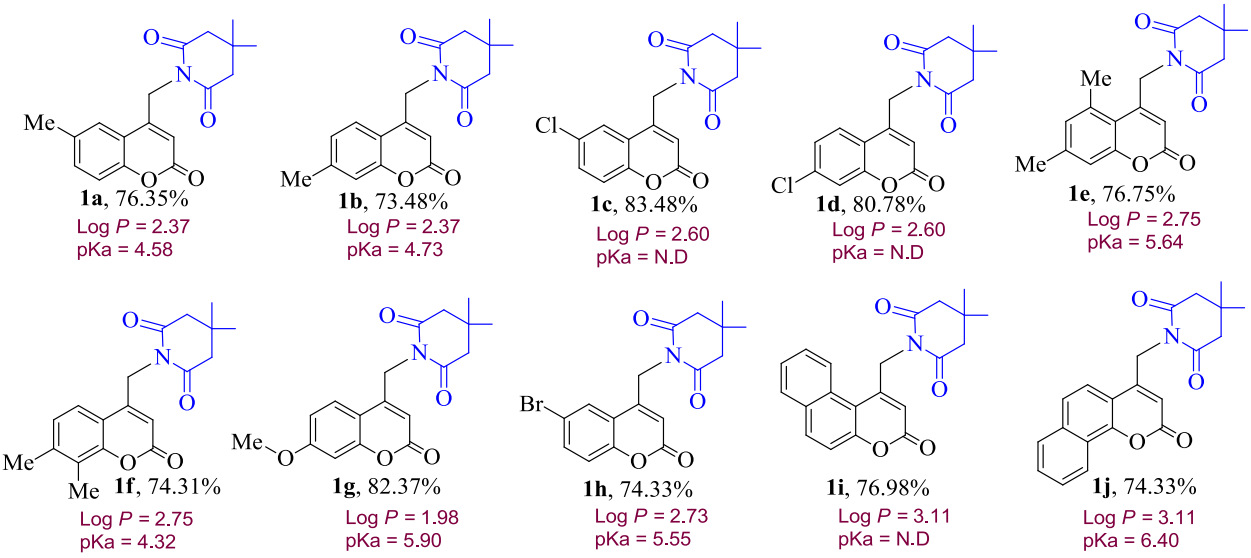


**Scheme 1.** Schematic representation to synthesize coumarin-cyclic imide derivatives (**1a-1j**)[a,b,c] [a]% yield of the purified products; [b]Log *P*: Calculated by http://www.molinspiration.com; [c]pKa: Calculated by potentiometric titration method; N.D: Not determined.

### 2.3. Antidiabetic activity studies

The coumarin-cyclic imide conjugates **(1a-1j)** were initially tested for their glucose uptake activity at 50 nM, 100 nM, 200 nM and 500 nM concentrations (Table 2). Different doses of compounds were given to the cells along with insulin resistant media for 24 h prior to the 2-NBDG uptake. Insulin resistant HepG2 cells treated with the test compounds showed increase in 2-NBDG (fluorescent glucose) uptake and the results are presented in Fig. 5. Compound **1f** and **1b** exhibited distinct activity with 85.21% and 80.89% of glucose uptake at 50 nM concentration respectively, which is comparable with standard antidiabetic drug Metformin (93.25% of glucose uptake). The second line of activity were observed by compounds **1e, 1h** and **1a** with 74.44%, 73.64% and 73.14% of glucose uptake respectively at 50 nM concentration.

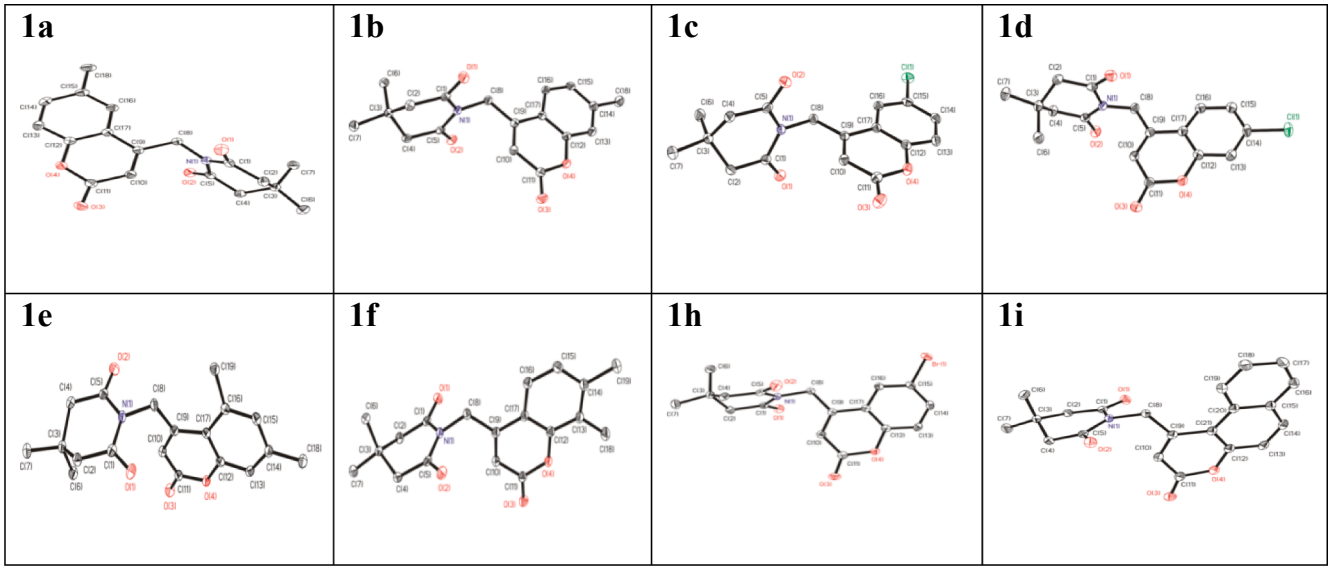


**Fig. 4.** ORTEP diagram for compounds **1a, 1b, 1c, 1d, 1e, 1f, 1h** and **1i**. All non-hydrogen atoms are represented by their 50% probability ellipsoids. Hydrogen atoms have been omitted for clarity purpose.

**Table 1**
Crystal Data and Structure Refinement for compounds **1a**, **1b**, **1c**, **1d**, **1e**, **1f**, **1h** and **1i**.

| | **1a** | **1b** | **1c** | **1d** |
|---|---|---|---|---|
| Formula | $C_{18}$ $H_{19}$ N $O_4$ | $C_{18}$ $H_{19}$ N $O_4$ | $C_{17}$ $H_{16}$ Cl N $O_4$ | $C_{17}$ $H_{16}$ Cl N $O_4$ |
| Formula weight | 313.34 | 313.34 | 333.76 | 333.76 |
| T, *K* | 100(2) | 100(2) | 100(2) | 100(2) |
| Wavelength, Å | 0.71073 | 0.71073 | 0.71073 | 0.71073 |
| Crystal system | Monoclinic | Monoclinic | Monoclinic | Monoclinic |
| Space group | C2/c | $P2_1/n$ | C2/c | $P2_1/c$ |
| *a*/Å | 18.7857(13) | 15.5791(7) | 18.6800(6) | 7.3640(2) |
| *b*/Å | 11.4459(9) | 5.7144(3) | 11.3537(3) | 15.5756(6) |
| *c*/Å | 14.6202(11) | 19.1011(9) | 14.6679(4) | 13.4200(5) |
| *α*/° | 90 | 90 | 90 | 90 |
| *β*/° | 94.156(4) | 111.790(2) | 94.0540(10) | 90.678(2) |
| γ/° | 90 | 90 | 90 | 90 |
| *V*/Å$^3$ | 3135.4(4) | 1578.98(13) | 3103.09(15) | 1539.15(9) |
| *Z* | 8 | 4 | 8 | 4 |
| $F_{000}$ | 1328 | 664 | 1392 | 696 |
| $D_{calc}$/g cm$^{-3}$ | 1.328 | 1.318 | 1.429 | 1.440 |
| *μ*/mm$^{-1}$ | 0.094 | 0.093 | 0.266 | 0.268 |
| *θ*/(°) | 2.17 to 27.18 | 2.82 to 26.40 | 2.10 to 26.42 | 2.00 to 26.41 |
| $R_{int}$ | 0.0293 | 0.0333 | 0.0257 | 0.0395 |
| Crystal size/mm$^3$ | 0.50 × 0.48 × 0.45 | 0.34 × 0.33 × 0.19 | 0.49 × 0.49 × 0.39 | 0.48 × 0.41 × 0.33 |
| Goodness-of-fit on $F^2$ | 1.050 | 1.055 | 1.033 | 1.036 |
| $R_1[I > 2\sigma(I)]$[a] | 0.0337 | 0.0345 | 0.0285 | 0.0367 |
| w$R_2$ (all data)[b] | 0.0943 | 0.0935 | 0.0781 | 0.1011 |
| Largest differences peak and hole (eÅ$^{-3}$) | 0.332 and −0.212 | 0.278 and −0.215 | 0.328 and −0.258 | 0.631 and −0.280 |
| | **1e** | **1f** | **1h** | **1i** |
| Formula | $C_{19}$ $H_{21}$ N $O_4$ | $C_{19}$ $H_{21}$ N $O_4$ | $C_{17}$ $H_{16}$ Br N $O_4$ | $C_{21}$ $H_{19}$ N $O_4$ |
| Formula weight | 327.37t | 327.37 | 378.22 | 349.37 |
| T, *K* | 100(2) | 100(2) | 100(2) | 100(2) |
| Wavelength, Å | 0.71073 | 0.71073 | 0.71073 | 0.71073 |
| Crystal system | Triclinic | Monoclinic | Monoclinic | Triclinic |
| Space group | P-1 | $P2_1/n$ | C2/c | P-1 |
| *a*/Å | 7.1642(3) | 17.0983(17) | 18.9597(6) | 12.4115(7) |
| *b*/Å | 9.2495(3) | 5.6965(6) | 11.3867(4) | 14.1571(8) |
| *c*/Å | 12.7646(5) | 17.4465(17) | 14.6964(5) | 19.8887(11) |
| *α*/° | 106.592(2) | 90 | 90 | 85.607(3) |
| *β*/° | 100.370(2) | 110.092(5) | 94.5580(10) | 82.596(3) |
| γ/° | 91.893(2) | 90 | 90 | 81.261(3) |
| *V*/Å$^3$ | 794.18(5) | 1595.9(3) | 3162.75(18) | 3419.5(3) |
| *Z* | 2 | 4 | 8 | 8 |
| $F_{000}$ | 348 | 696 | 1536 | 1472 |
| $D_{calc}$/g cm$^{-3}$ | 1.369 | 1.363 | 1.589 | 1.357 |
| *μ*/mm$^{-1}$ | 0.096 | 0.096 | 2.619 | 0.094 |
| *θ*/(°) | 2.90–26.40 | 2.06–26.41 | 2.16–26.41 | 1.03–26.52 |
| $R_{int}$ | 0.0213 | 0.0226 | 0.0260 | 0.0415 |
| Crystal size/mm$^3$ | 0.49 × 0.45 × 0.42 | 0.47 × 0.45 × 0.44 | 0.46 × 0.41 × 0.33 | 0.46 × 0.41 × 0.39 |
| Goodness-of-fit on $F^2$ | 1.049 | 1.083 | 1.077 | 1.060 |
| $R_1[I > 2\sigma(I)]$ [a] | 0.0334 | 0.0336 | 0.0209 | 0.0366 |
| w$R_2$ (all data) [b] | 0.0881 | 0.1040 | 0.0504 | 0.1012 |
| Largest difference peak and hole (eÅ$^{-3}$) | 0.313 and −0.218 | 0.303 and −0.239 | 0.389 and −0.440 | 0.243 and −0.273 |

**Table 2**
Glucose uptake by insulin resistant liver hepatocyte carcinoma (HepG2) cells.

| Compound | % of glucose uptake by HepG2 cells at 50–500 nM concentration | | | |
|---|---|---|---|---|
| | 50 nM | 100 nM | 200 nM | 500 nM |
| **1a** | 73.14% | 79.26% | 81.56% | 83.17% |
| **1b** | 80.89% | 85.31% | 88.38% | 90.86% |
| **1c** | 70.17% | 84.28% | 85.41% | 90.62% |
| **1d** | 68.21% | 74.98% | 87.36% | 88.38% |
| **1e** | 74.44% | 79.05% | 80.00% | 81.57% |
| **1f** | 85.21% | 87.68% | 89.67% | 91.76% |
| **1g** | 72.08% | 85.56% | 86.45% | 87.47% |
| **1h** | 73.64% | 84.69% | 85.37% | 87.04% |
| **1i** | 65.80% | 67.37% | 70.58% | 78.57% |
| **1j** | 71.00% | 78.11% | 83.96% | 87.16% |
| **Metformin** | 93.25% | N.D | N.D | N.D |

N.D – Not Done.

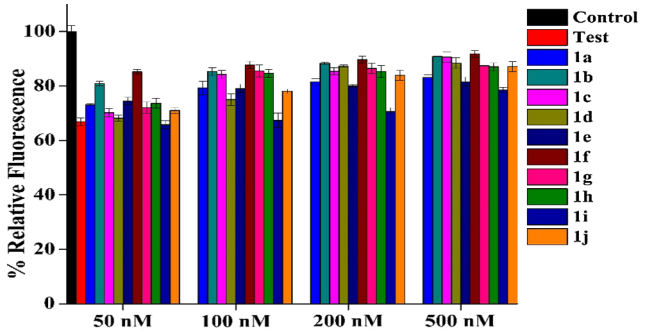


**Fig. 5.** Antidiabetic activity for compounds **(1a-1j)**, assessed by 2-NBDG uptake assay which gave the % of glucose uptake by insulin resistant HepG2 cells at 50, 100, 200 and 500 nM concentration of compounds.

Compounds **1c, 1d, 1g, 1i** and **1j** showed moderate activity in the range of 65.80–72.08 % at 50 nM concentration. It was noted that even at higher doses (100–500 nM), there was no significant change in the NBDG uptake (Table 2); which suggest that the compounds were active at minimal dose concentration. From structural point of view, it was noted that *7,8 di-$CH_3$* substituted coumarin (**1f**) was found to be highly active with exceptional glucose uptake of 85.21%. The next line of activity was observed by *–$CH_3$* substituent at C-7 position (**1b**) with 80.89% followed by *5,7 di-$CH_3$* substituent (**1e**) with 74.44% of glucose uptake at 50 nM concentration. The *-Br* substituent at C-6 position (**1h**) and *–$CH_3$* substituent at C-6 position (**1a**) obtained comparable activity with 73.64 and 73.14% of glucose uptake respectively. The compound with *–Cl* substituent at C-6 (**1c**) and C-7 (**1d**) position showed 70.17% and 68.21% of glucose uptake respectively. The *−$OCH_3$* substituted at C-7 position (**1 g**) of the coumarin ring showed 72.08% of glucose uptake. Whereas *5,6 Benzo* (**1i**) and *7,8 Benzo* (**1j**) substituted coumarin derivatives showed 65.80% and 71.00% of glucose uptake respectively. Overall it was observed that *−$CH_3$* substituted compounds were found to be more favourable candidates for enhancing the activity.

### 2.4. Correlation between X-ray crystal structure and antidiabetic activity

A notable observation was illustrated from X-ray crystal studies that compounds **1f** and **1b** which exhibited excellent glucose uptake of 85.21 and 80.89% respectively have shown C═O-π interactions (Fig. 6). The X-ray crystal packing diagram for **1f** and **1b** is given in supporting information (See page no. S23, Fig. S20). To visualize these aspects, atropoisomers images for **1f** and **1b** have been depicted in supporting information (See page no. S24, Fig. S21). Compounds **1a**, **1c**, **1d**, **1e**, **1h** and **1i** which demonstrated moderate glucose uptake have shown π-π interactions between coumarin rings (See page no. S25, Fig. S22 in supporting information). The atropoisomers images for compounds **1a**, **1c**, **1d**, **1e**, **1h** and **1i** are depicted in supporting information (See page no. S25, Fig. S23). The enhanced activities exhibited by **1f** and **1b** can be related with the dihedral angles between the plane that cuts in half the cyclic imides and the plane defined for the coumarin ring atoms by rotation around the C8-C9 link. This theoretical evidence clearly indicates that there is structural correlation between the structural angle (dihedral angle) and antidiabetic activity of the compound. The obtained results may serve in future to predict the bioactivity of the compounds through single crystal X-ray studies.

### 2.5. Toxicity study against healthy cells

Compounds were evaluated against Human Embryonic Kidney cells (HEK293) to check the safety profile. Their toxicity levels were evaluated through MTT assay. The results (Fig. 7) indicated that none of the compounds showed any significant toxicity against HEK293 cells at 50, 100, 500 and 1000 nM concentration, suggesting great potential for their *in-vivo* use as antidiabetic agents. It was found that, when the cells were treated with compounds **1a-1h** and **1j**, the % survival of HEK293 cells were well above 85% at 50 nM, above 80% at 500 nM and above 65% at 1000 nM concentration. This clearly indicates that the compounds were well within the toxicity limits and thereby exhibited good safety profile. An exception was compound **1i** which showed moderate cytotoxicity with 84, 67 and 59% survival of HEK293 cells at 50, 500 and 1000 nM concentration respectively. It is noteworthy to mention that compound **1f** and **1b** which showed significant glucose uptake also revealed remarkable safety profile with 94 and 68% survival of HEK293 cells at 1000 nM concentration respectively, signifying that they have a high prospective for *in-vivo* use as antidiabetic agents.

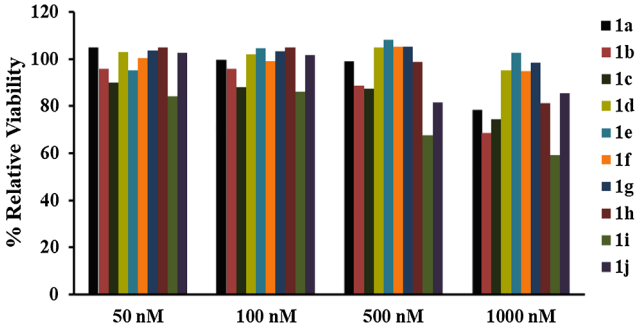


**Fig. 7.** Cytotoxicity study of compounds (**1a-1j**) at 50 to 1000 nM concentration against Human Embryonic Kidney cells (HEK293) by MTT assay.

Further, to evaluate the drug like properties of the compounds, physicochemical studies were performed (http://www.molinspiration.com) to calculate important pharmacological properties like log *P*, polar surface area, number of hydrogen bond donors and acceptors. All the compounds were found to follow Lipinski rule of five (RO5) [32] according to which, molecular weights were below 500 Da, lipophilicity expressed as a log*P* was less than 5 (Scheme 1); the number of hydrogen bond donors as well as acceptors were also less than 5. The results clearly indicates that none of the compounds violate the rules and they fall well within the range as stated by the RO5 to qualify as a drug candidate [32,33].

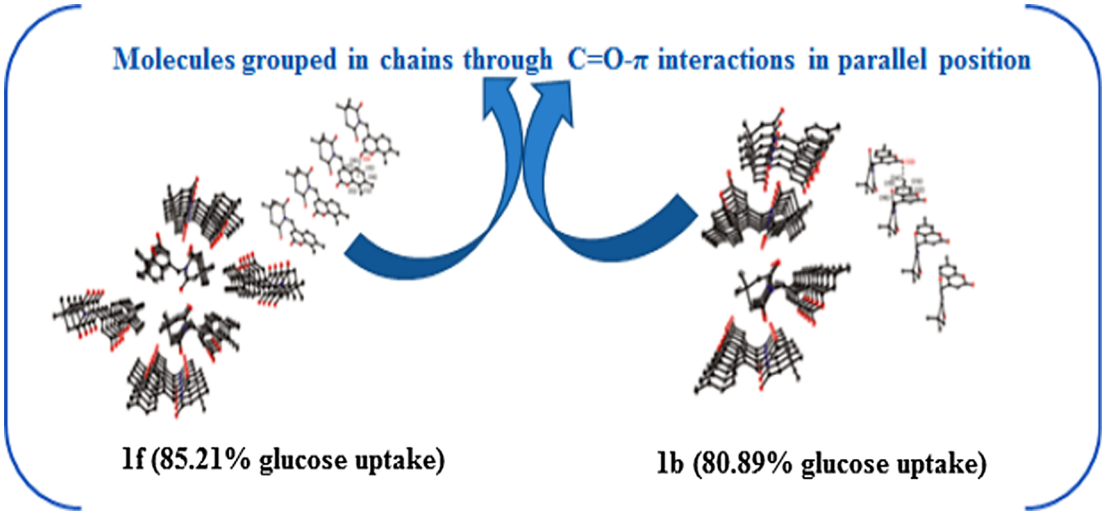


**Fig. 6.** Compounds having C═O–π interactions exhibited significant antidiabetic activity.

### 2.6. Solution stability studies

The physical and chemical properties of bio-active compounds such as hydrophobicity and tissue penetrability are significantly dependent on their $pK_a$ value. To determine the $pK_a$ of the newly synthesized coumarin-cyclic imide conjugates, potentiometric titration method was employed. Further, UV–Visible spectroscopic technique was employed at varied pH ≈ (3.4–8.7) conditions [37] to check the stability of active compounds. Initially, pH of active compounds **1a, 1b, 1e, 1f, 1g, 1h** and **1j** ($10^{-4}$ M each) were in the range 6.9–7.6 and this pH was steadily brought down to acidic (pH ~ 3) by titration with HCl (25 mM). After attaining pH ~ 3, the acidic solution was further titrated with KOH (25 mM) till pH reached basic (pH ~ 9). Thereby, through this process, pH variation trend was prudently studied and a graphical plot of volume of KOH added vs pH was drawn. From the obtained equivalence point, $pK_a$ values were calculated (see Figs. S1–S7 in Supporting Information). The $pK_a$ values of the tested compounds were found to be in between 4.3 and 6.4 (Scheme 1), which suggest that the newly synthesized compounds have capability to cross the biological membranes [38].

In order to evaluate the solution stability of active compounds (**1a, 1b, 1e, 1f, 1g, 1h** and **1j**), UV–Visible absorption analysis was done in the pH range of 3.4 to 8.7. For example, in case of compound **1f** initial pH = 7, was brought to acidic pH by slowly titrating with HCl (25 mM) which resulted in the increased intensity of the absorption band at 330 nm. The addition of HCl was continued until pH reached 3.4 (pH = 7.0 to 3.4, given in Fig. 8(A)). The solution reaction was found to be reversed from pH 3.4 by slowly titrating with KOH (25 mM) (pH = 3.4 to 8.3, given in Fig. 8(B)). From Fig. 8(B), it could be seen that absorbance bands retained their peak positions during the experiments and no additional bands were detected which clarifies that compound **1f** is stable at varied pH conditions.

Similarly, for other active compounds (**1a, 1b, 1e, 1g, 1h and 1j**) stability studies were established in the pH range 3.5–8.7 (see Figs. S8–S19 in Supporting Information).

### 2.7. HSA interaction study

Assessment of the bioavailability of a prospective drug is of utmost importance and in this direction; plasma protein binding study plays a highly decisive role. It is one of the crucial steps involved before screening the potential therapeutic agent *in*-vivo [39]. One such important plasma protein is human serum albumin (HSA) which is not only abundantly present in plasma (60% of total plasma protein), but also is a transporter of metabolic compounds and drug molecules in body. It can act as a reserve for drug molecules and allow for passive targeting due to its preferential uptake in diseased tissues and cells [40]. The study of human serum albumin binding will help for further prediction of the pharmacokinetics of a prospective drugs. Interaction of the most active compound **1f** with HSA was studied using a combination of fluorescence, UV–Visible spectroscopic techniques and *in-silico* modeling study.

#### 2.7.1. Steady-state fluorescence quenching studies

HSA has intrinsic fluorophore residues such as tryptophan and tyrosine which mainly emits at around 340 nm when excited at about 280 nm [41]. This emission is sensitive to the environment around the protein and hence can provide information about the binding of compound with HSA. The emission spectra of HSA (5 μM) at various concentrations of **1f** (0.83–8.19 μM) in pH 7.4 phosphate buffer were recorded at three different temperatures, *viz.* 298 K, 303 K and 308 K. At all the temperatures, the emission maxima which were observed at 337 nm got steadily quenched upon successive addition of **1f** (see Fig. 9A).

To evaluate the type of quenching of fluorophore HSA by the quencher **1f**, Stern-Volmer plot ($F_0$/F vs [Q]) was plotted using Eq. (1) [42].

$$\frac{F_0}{F} = 1 + k_q \tau_0 [Q] = 1 + K_{SV}[Q] \quad (1)$$

where $F_0$ and F are the emission intensities of pure HSA and HSA added with different concentrations of **1f** respectively. *kq* is the rate constant of the biomolecular quenching reaction and *Ksv*, the Stern-Volmer quenching constant. $\tau_0$ is the average lifetime of molecules of HSA protein (≈ $5 \times 10^{-9}$ s) [41] and [Q] is the concentration of quencher compound **1f**. Fig. 9B gives the Stern-Volmer plot at different temperatures. All the SV plots gave almost linear graphs with $R^2$ in the range of 0.998–0.999. The values of $K_{SV}$ and $k_q$ (Table 3) show that the quenching constants increase with increasing temperature thereby suggesting dynamic or collisional quenching [42].

To find the number of binding site(s) in the protein for the compound **1f**, a double log graph of log [($F_0$–F)/F] vs log [Q] (Fig. 10A) was drawn and using equation (2), the value of binding sites (*n*) and binding constant ($K_a$) was calculated at different temperatures.

$$log\left(\frac{F_0 - F}{F}\right) = logK_a + nlog[Q] \quad (2)$$

The values obtained are given in Table 4 which suggest that there is one binding site in the protein for **1f** and that the binding between compound and HSA is strong.

The thermodynamics involved in the binding reaction of **1f** and HSA was evaluated by drawing the van't Hoff's plot (Fig. 10B) from which the thermodynamic parameters, change in enthalpy (*ΔH*) and change in

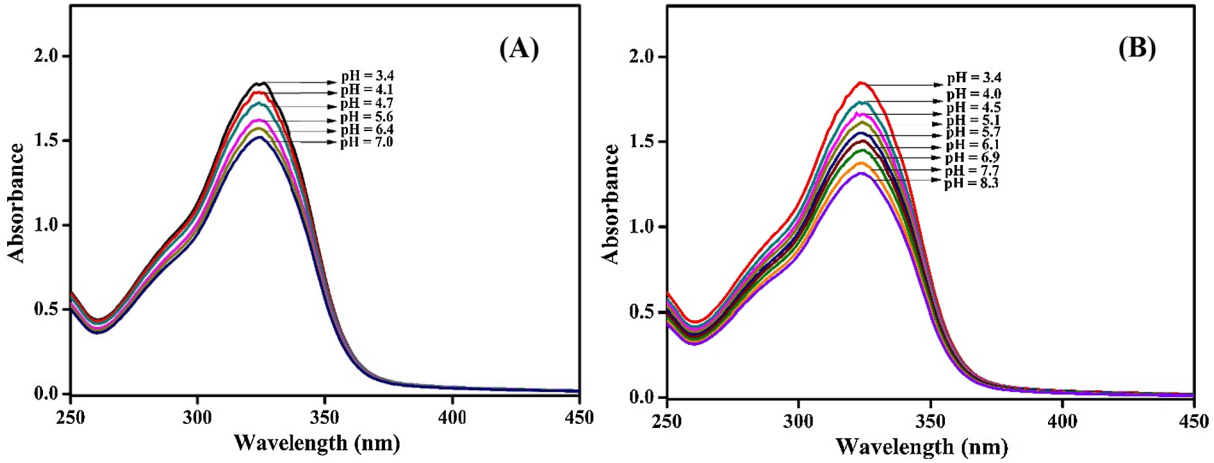


**Fig. 8.** UV–Visible titration study of compound **1f** ($10^{-4}$ M) with HCl (25 mM) (A) and KOH (25 mM) (B).

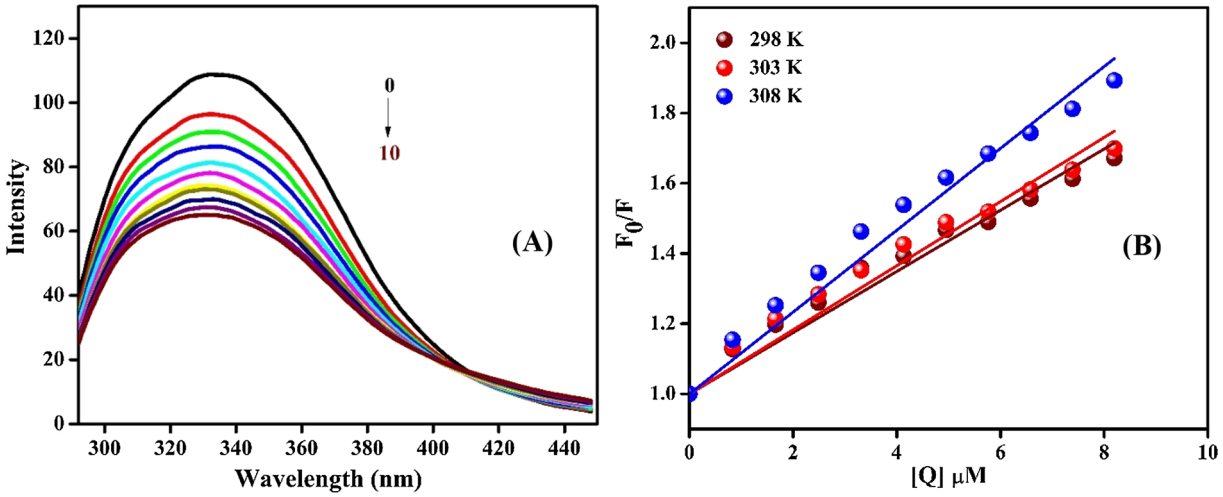


**Fig. 9.** (A) Intrinsinc fluorescence quenching study of HSA at 298 K with the titration of compound **1f** at ten different concentrations; (B) Stern-Volmer plot obtained from the quenching study at three temperatures from which quenching constants were calculated.

**Table 3**
Stern–Volmer quenching constants ($K_{sv}$) and biomolecular quenching rate constant ($k_q$) of HSA-**1f** system at three temperatures.

| Temp (K) | $K_{sv}$ (L mol$^{-1}$) | $k_q$ (L mol$^{-1}$ s$^{-1}$) | $R^2$ | SD |
|---|---|---|---|---|
| 298 | $8.72 \times 10^4$ | $1.74 \times 10^{13}$ | 0.9990 | 0.0026 |
| 303 | $9.13 \times 10^4$ | $1.83 \times 10^{13}$ | 0.9989 | 0.0028 |
| 308 | $11.66 \times 10^4$ | $2.33 \times 10^{13}$ | 0.9988 | 0.0032 |

entropy ($\Delta S$) were calculated using the van't Hoff's Eq. (3).

$$lnK_a = -\frac{\Delta H}{RT} + \frac{\Delta S}{R} \quad (3)$$

The Gibb's free energy change ($\Delta G$) at different temperatures were calculated using the Gibb's free energy relation (Eq. (4))

$$\Delta G = \Delta H - T\Delta S \quad (4)$$

The obtained thermodynamic parameters suggest that the interaction between **1f** and HSA is mainly governed through hydrophobic forces and that the compound **1f** is mainly surrounded by hydrophobic amino acid residues. As it can be seen from Table 4, the value of $\Delta G$ was observed to be negative at all the studied temperatures which showed the spontaneity in the interaction process [43].

### 2.7.2. Synchronous and 3D fluorescence studies

Synchronous fluorescence technique can differentiate between the fluorescence profiles of amino acid residues like tyrosine and tryptophan and gathers information on HSA vicinity and environment [44]. Synchronous fluorescence was recorded between $\lambda_{em}$ = 290–500 nm and $\lambda_{exc}$ = 200–350 nm in the wavelength interval of $\Delta\lambda$ = 15 nm and $\Delta\lambda$ = 60 nm with respect to tyrosine and tryptophan amino acids respectively. A higher % of quenching of the tryptophan fluorescence was observed (Fig. 11A and B).

Three dimensional fluorescence spectroscopy (Fig. 12) helps to simultaneously determine the excitation and emission profile of protein and hence examines the quenching pattern in a more reliable way [45]. The 3D spectra of HSA (5 μM) upon titration with an optimal concentration of **1f** (8.20 μM) were analysed in the wavelength range of $\lambda_{em}$ = 200–650 nm and $\lambda_{exc}$ = 200–360 nm at a scan rate of 600 nm/min and wavelength increment, $\Delta\lambda$ = 2 nm.

Fig. 12A and B represent the 3D fluorescence spectra and the respective contour diagrams of pure HSA and HSA-**1f** adduct respectively. Peak **a** is a representation of 1st order Rayleigh scattering ($\lambda_{em} = \lambda_{ex}$) and peak **b** is a representation of 2nd order Rayleigh scattering ($\lambda_{em} = 2\lambda_{ex}$). Peak **1** and peak **2** are due to the $\pi \rightarrow \pi^*$ transitions of the aromatic amino acids, mainly, Trp residues of protein and the typical

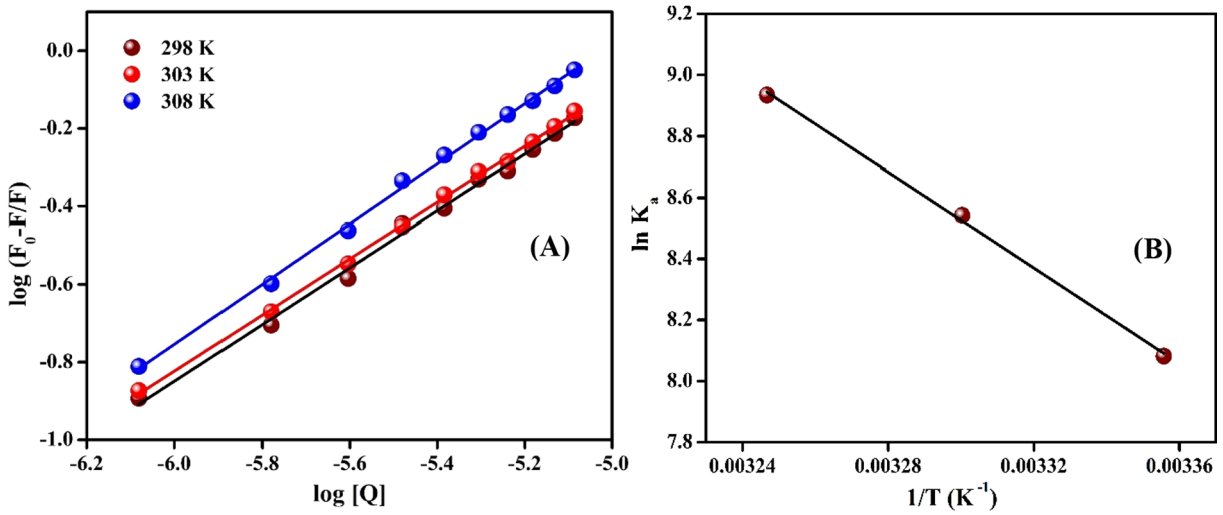


**Fig. 10.** (A) Double log graph to calculate the binding sites and binding constants at different temperatures; (B) van't Hoff's plot to find out thermodynamic parameters $\Delta H$, $\Delta S$ and $\Delta G$.

**Table 4**
The binding constants ($K_a$), binding site ($n$) and thermodynamic parameters of HSA and **1f** interaction at three temperatures.

| Temp (K) | $K_a$ (L mol$^{-1}$) | n | $R^2$ | SD | $\Delta H^0$ (kJ M$^{-1}$) | $\Delta S^0$ (J M$^{-1}$ K$^{-1}$) | $\Delta G^0$ (kJ M$^{-1}$) |
|---|---|---|---|---|---|---|---|
| 298 | $3.23 \times 10^3$ | 0.72 | 0.9986 | 0.0501 | 65.06 | 285.59 | −20.04 |
| 303 | $5.13 \times 10^3$ | 0.73 | 0.9949 | 0.0960 | | | −21.47 |
| 308 | $7.59 \times 10^3$ | 0.77 | 0.9979 | 0.0635 | | | −22.90 |

n → π* transition due to the peptide backbone respectively [46]. Both peak **1** and peak **2** got quenched with the peak **1** getting extensively quenched. The weakening intensity observed for peaks **1** and **2** upon addition of compound **1f** (Table 5) concludes that there occurs a gradual unfolding of HSA peptide chain which causes conformational changes in HSA.

The synchronous and 3D fluorescence studies, in combination, signify that during the process of interaction with HSA, compound **1f** causes relatively greater quenching of tryptophan than other amino acid residues by inducing gradual changes in the protein's secondary conformational structure.

### 2.7.3. UV–Visible and FRET study

The extent of binding between a drug molecule and a biomacromolecule like HSA can be further investigated using UV–Visible absorption spectroscopy [47]. HSA exhibits absorption maxima at around 280 nm [48] which is observed as an important factor in analysing the binding between HSA and the quencher compound. The absorption spectra of HSA (5 μM) upon titration with various concentrations of compound **1f** (0.83–8.19 μM) in pH 7.4 phosphate buffer at 298 K is shown in Fig. 13A. With increasing concentrations of **1f**, the pattern of absorbance showed an increasing trend. FRET phenomenon was checked to find out the distance of vicinity at which the quencher acceptor compound **1f** lies from the fluorophore donor HSA. Forster resonance energy transfer (FRET) occurs when there is transfer of electromagnetic energy non-radiatively from a fluorophore donor to a vicinal quencher acceptor molecule [49]. Fig. 13B represents the spectral overlap between the fluorescence emission of HSA and the absorption spectrum of **1f**. Efficiency of energy transfer (E) between **1f** and HSA can be found out using the Forster non-radiative energy transfer theory [48] according to the Eq. (5).

$$E = 1 - \frac{F_0}{F} = \frac{R_0^6}{R_0^6 + r^6} \tag{5}$$

where r is the vicinity between binding sites of HSA and **1f** and $R_0$ is the Förster critical energy transfer distance for 50% efficiency of energy transfer. $R_0$ is calculated using Eq. (6).

$$R_0^6 = 8.79 \times 10^{-25} K^2 N^{-4} \Phi J \tag{6}$$

where $K^2$ is the factor of spatial orientation for HSA = 2/3, N is the average refractive index of the medium = 1.36, ϕ is the HSA fluorescence quantum yield = 0.15 [50] and J is the integral of overlap between the emission spectrum of HSA and absorption spectrum of **1f** which can be calculated using Eq. (7).

$$J = \frac{\int_0^\infty F(\lambda) \in (\lambda) \lambda^4 d\lambda}{\int_0^\infty F(\lambda) d\lambda} \tag{7}$$

where F(λ) is the corrected emission intensity of HSA over the wavelength range (λ + dλ) to λ and ε(λ) is the molar extinction coefficient of **1f** at λ [51]. The values of r, $R_0$, J and E were found to be 2.44 nm, 2.82 nm, $1.97 \times 10^{-14}$cm$^3$/L/mol and 0.71 respectively. It was found that the values (0.5 $R_0$ < r < 1.5 $R_0$) are in agreement with the conditions laid by FRET theory [51] which indicates energy transfer probability between HSA to **1f** to be high [52]. The UV–Visible and FRET studies suggest effective collision between **1f** and HSA and that the proximity of protein from **1f** is very close which induces favourable transfer of energy between **1f** and HSA during their interaction.

### 2.7.4. Competitive binding study with site markers

To evalaute the specific binding pocket of HSA for **1f** binding, two known anti-inflammatory drugs were used as site markers, *viz.* Indomethacin (IND) and Ibuprofen (IBU). It is known that the hydrophobic binding pockets of HSA are situated at subdomains IIA and IIIA respectively. These drugs specifically bind to site I and II located in the subdomains II and III of HSA respectively [53]. For this study, the intrinsinc fluorescence of HSA, HSA-IND and HSA-IBU systems were first measured. The effect of the addition of successive concentrations of compound **1f** on their fluorescence profile was studied. As seen in the Fig. 14A, the addition of **1f** to HSA-IND system drastically decreases the

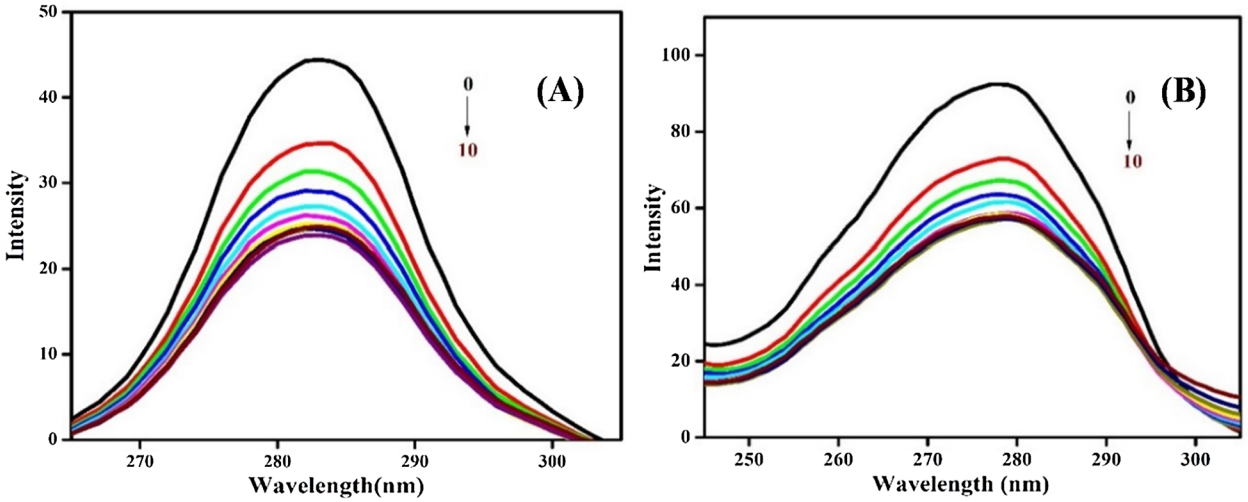


**Fig. 11.** Synchronous fluorescence measurement of HSA fluorophore upon addition of compound **1f** which measures fluorescence given out by (A) tyrosine residue at Δλ = 15 nm and (B) tryptophan residue at Δλ = 60 nm.

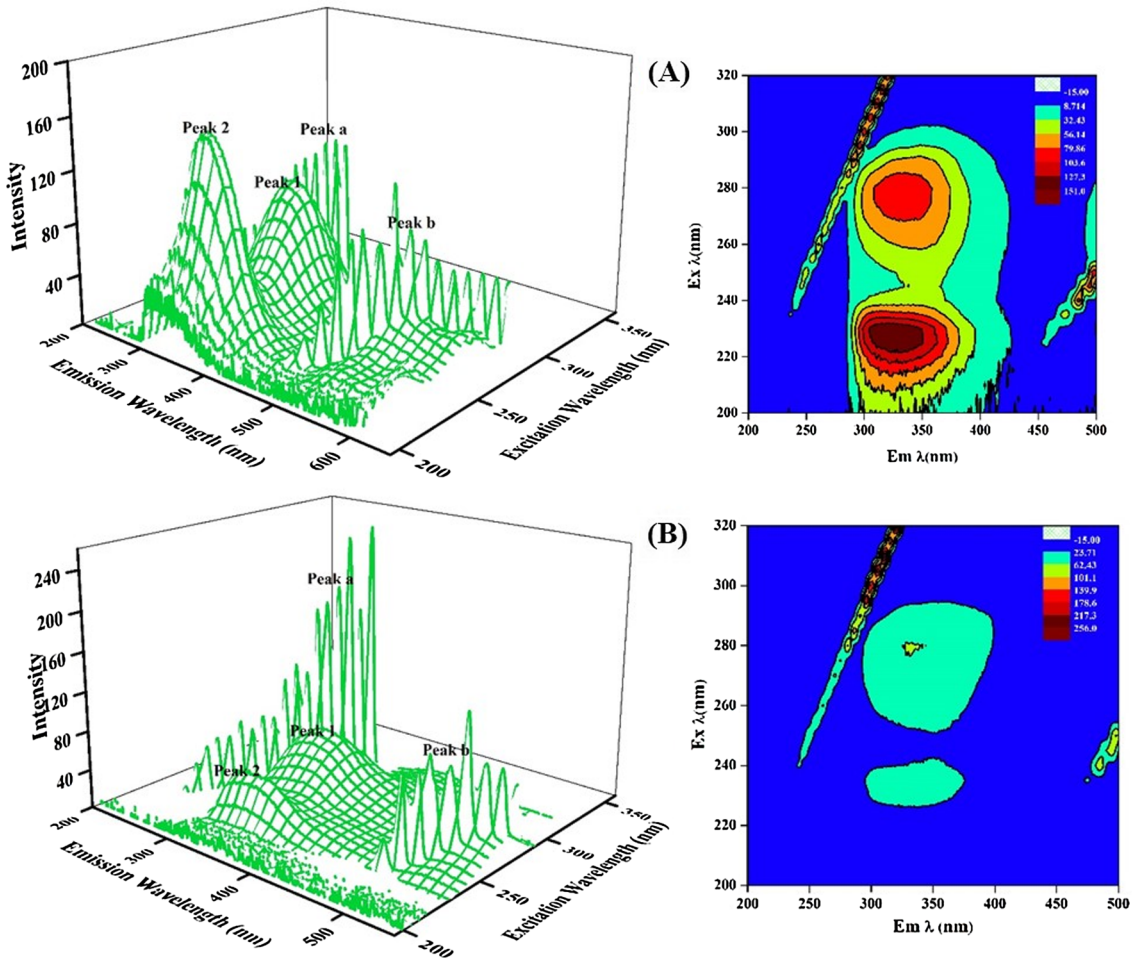


**Fig. 12.** Three dimensional fluorescence spectra and the respective contour diagrams of (A) pure HSA; (B) HSA titrated with **1f**.

**Table 5**
Peak **1**, peak **2** changes observed from 3 dimensional fluorescence study.

| Samples | Peak 1 | | | Peak 2 | | |
|---|---|---|---|---|---|---|
| | $\lambda_{ex}/\lambda_{em}$ (nm) | Intensity | Stokes shift $\Delta\lambda$(nm) | $\lambda_{ex}/\lambda_{em}$ (nm) | Intensity | Stokes shift $\Delta\lambda$ (nm) |
| HSA | 280/334 | 95 | 54 | 225/327 | 150 | 102 |
| HSA + **1f** | 280/333 | 64 | 53 | 225/337 | 20 | 112 |

fluorescence, with the intenisty much lower than that observed in HSA-**1f** system without the IND marker which suggests that there was a competition between **1f** and IND and that site I marker Indomethacin interfered with the binding of **1f** to HSA. On the contrary, when **1f** was added to the HSA-IBU system (Fig. 14B), the fluorescence reduced gradually and the intensity recorded were nearly same as that measured in the HSA-**1f** system without the marker which indicates that site II marker did not interfere with the binding of **1f** to HSA. The results obtained summarize that site I marker Indomethacin competes with **1f** for binding with HSA thereby suggesting that the compound **1f** binds to the hydrophobic pocket IIA of HSA. The molecular docking/*in-silico* study also corroborates with this conclusion.

### *2.7.5. In-silico study*

Molecular docking study of compound **1f** with HSA was done to investigate the intermolecular interactions between **1f** and various amino acid residues of HSA. HSA structure consists of three large homologous domains which are numbered as I (residues 1–195), II (196–383) and III (384–585). All the three domains comprise of sub-domains A and B. The ligand binding hydrophobic pockets of site I and II are respectively situated at sub domains IIA and IIIA [41]. **1f** binds with the subdomain IIA of HSA (Fig. 15). Compound **1f** was found to be adjacent to the hydrophobic residues of HSA such as, TRY150, GLU153, SER192, LYS195, GLN196, LYS199, TRP214, LEU219, ARG222, LEU238, HIS242, ARG257, LEU260, ALA261, ILE264, SER287, HIS288, ILE290, ALA291 and GLU292 (Fig. 15). Compound **1f** got accommodated in the cavity adjacent to TRP214 residue and therefore had a good and favourable interactive profile inside the cavity [54]. Four hydrogen bonds were found between **1f** and GLN196, LYS199, ARG222 and ARG257 residue of HSA. Molecular docking results suggested that the main force involved in binding of **1f** with HSA is hydrophobic interaction, whereas hydrogen bonds might have a minor contribution in the interaction between **1f** and HSA.

## 3. Experimental section

### *3.1. Materials and methods*

All the chemicals and reagents procured were of analytical grade and were used directly without purification. The completion of reaction was confirmed using TLC (Thin layer chromatography) by visualizing the spots under ultraviolet light (254 nm). To run the TLC, ethyl acetate: hexane (20: 80) mobile phase system was used. Melting point of the compounds were determined on a Buchi apparatus in open capillary tubes. $^{1}H$ and $^{13}C$ NMR spectra were recorded on a Bruker

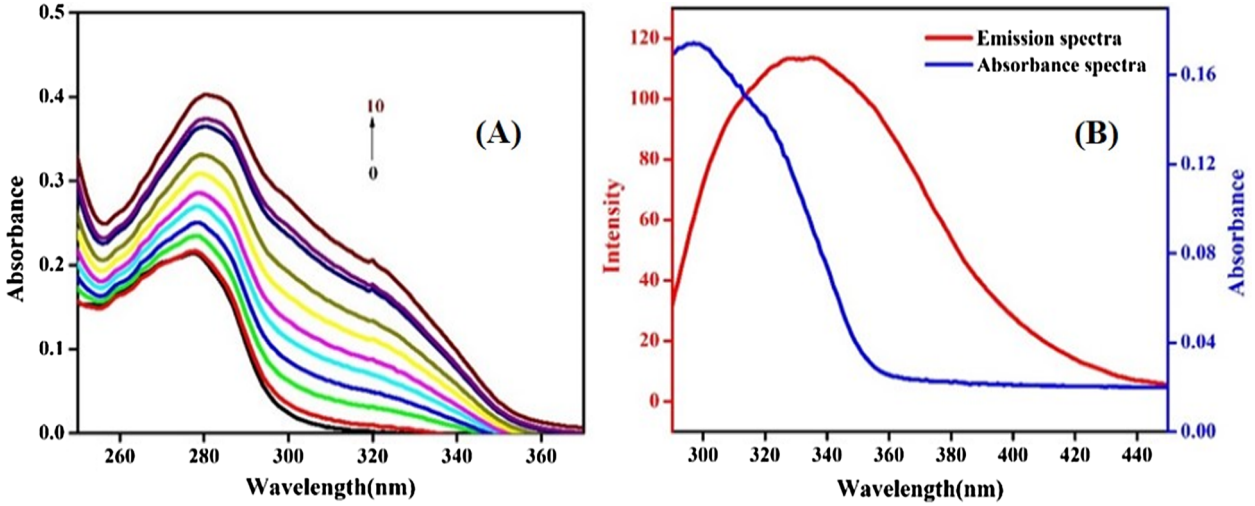


**Fig. 13.** (A) Absorption spectra of HSA with the titration of increasing concentration of compound **1f**; (B) A representation of the overlap between the absorption spectrum of **1f** and fluorescense emission spectrum of HSA.

400 MHz spectrometer using $CDCl_3$ as solvent. All chemical shifts were reported as $\delta$ values (ppm). Mass spectra were recorded using Shimadzu GCMSQP2010S. IR spectra were recorded on a Nicolet Impact 410 FTIR spectrometer using KBr pellets. The elemental analysis was carried out using Euro Vector E-3000 system. UV–Visible spectral data were recorded on a Shimadzu, UV-1800 instrument. X-ray diffraction analysis data for compounds **1a, 1b, 1c, 1d, 1e, 1f, 1h** and **1i** were recorded on a Bruker SMART Apex CCD diffractometer. SHELXTL program was used to record complex scattering factors. Potentiometric titration experiments were carried on a pH meter (HI5000 Series, Hanna).

### 3.2. Protocol to synthesize coumarin-cyclic imide conjugates (1a − 1j)

4,4-Dimethylpiperidine-2,6-dione (1.41 g, 10 mM) was dissolved in dry acetone (10 mL) in the presence of anhydrous $K_2CO_3$ (4.14 g, 30 mM). The reaction mixture was kept for stirring (30 min at 50 °C) and then substituted 4-bromomethyl coumarin (**a-j**, 10 mM) was added. The reaction mixture was kept for stirring at 55–60 °C temperature for 10 h. The progress of the reaction was monitored using TLC. Once the reaction was complete, the solution was gradually cooled to room temperature and quenched with crushed ice. The solid product obtained was further recrystallized with ethanol and dried in *vacuo*. Elemental analysis, NMR ($^1$H and $^{13}$C), IR and GC–MS data for all the compounds corroborate with their formulation.

### 3.3. Data for compounds (1a-1j)

**4,4-dimethyl-1-((6-methyl-2-oxo-2H-chromen-4-yl)methyl)piperidine-2,6-dione (1a) [$C_{18}H_{19}NO_4$].** 4-(bromomethyl)-6-methyl-2H-chromen-2-one **(a)**: 2.53 g, 10 mM; Yield: 2.39 g (76.35%); colourless crystals; m.p. 285 – 286 °C; Anal. calcd. for. $C_{18}H_{19}NO_4$: C, 68.99; H, 6.11; N, 4.47. Found: C, 68.97; H, 6.13; N, 4.46; ATR-IR ($\nu_{max}$/cm$^{-1}$): 1716 (C═O of lactone), 1667 (Cyclic C═O); $^1$H NMR (400 MHz , $CDCl_3$, $\delta$ ppm) 1.14 (s, 6H, –$CH_3$), 2.39 (s, 3H, –$CH_3$), 2.62 (s, 4H, –$CH_2$), 5.10 (s, 2H, –$CH_2$), 5.90 (s, 1H, –CH), 7.20–7.24 (m, 1H, Ar-H), 7.31–7.34(m, 1H, Ar-H), 7.42 (s, 1H, Ar-H); $^{13}$C NMR (100 MHz, $CDCl_3$, δ ppm): 16.22, 23.12, 23.22, 24.54, 34.21, 41.38, 106.82, 112.25, 112.75, 118.70, 128.22, 129.26, 144.94, 146.91, 155.85, 166.75; GC–MS: 313 [M]$^+$.

**4,4-dimethyl-1-((7-methyl-2-oxo-2H-chromen-4-yl)methyl)piperidine-2,6-dione (1b) [$C_{18}H_{19}NO_4$].** 4-(bromomethyl)-7-methyl-2H-chromen-2-one (b): 2.53 g, 10 mM; Yield: 2.30 g (73.48%), colourless crystal; mp 293–294 °C; Anal. calcd. for. $C_{18}H_{19}NO_4$: C, 68.99; H, 6.11; N, 4.47. Found: C, 68.96; H, 6.09; N, 4.45; ATR-IR ($\nu_{max}$/cm$^{-1}$):

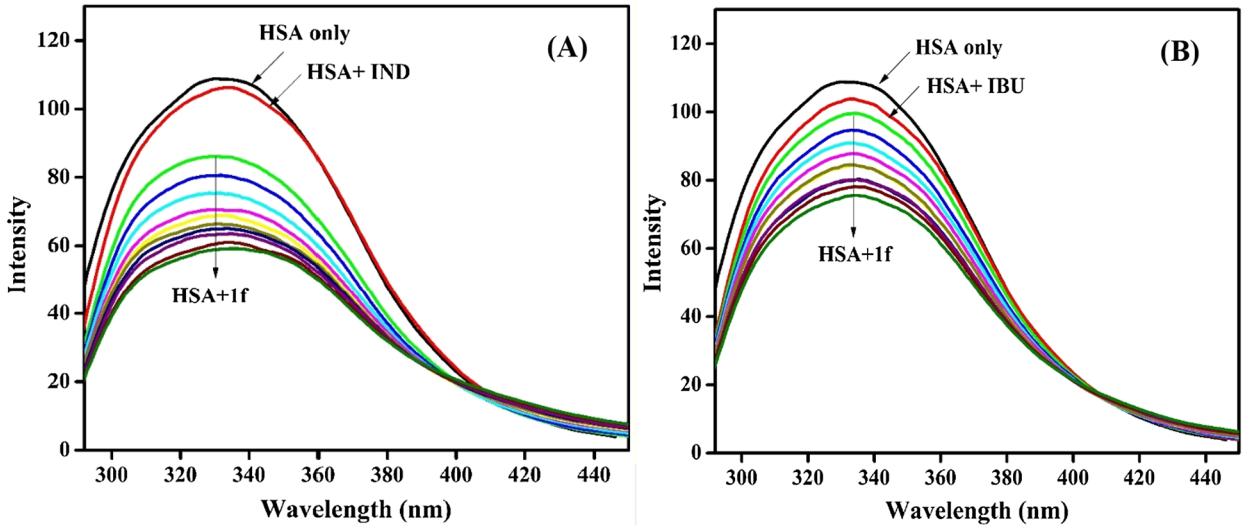


**Fig. 14.** Depiction of HSA binding site competitive study (A) For HSA-IND-**1f** system and (B) For HSA-IBU-**1f** system.

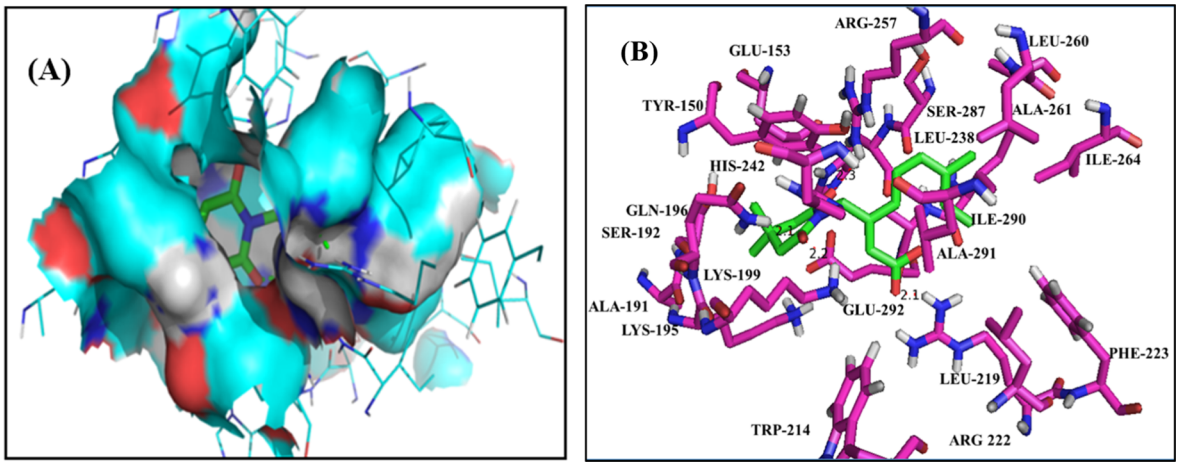


**Fig. 15.** (A) Representation of docked **1f** into HSA at the pocket site (B) Docked **1f** (represented by green coloured sticks) and neighbouring amino acid residues (represented by magenta coloured sticks) of HSA.

1718 (C═O of lactone), 1663 (Cyclic C═O); $^{1}$H NMR (400 MHz , $CDCl_3$, $\delta$ ppm) 1.14 (s, 6H, –$CH_3$), 2.43 (s, 3H, –$CH_3$), 2.62 (s, 4H, –$CH_2$), 5.10 (s, 2H, –$CH_2$), 5.87 (s, 1H, –CH), 7.10–7.13 (m, 2H, Ar-H), 7.52(d, 1H, $J$ = 8.0 Hz); $^{13}$C NMR (100 MHz, $CDCl_3$, δ ppm): 21.61, 27.95, 29.30, 38.95, 46.14, 110.71, 115.39, 117.45, 123.28, 125.54, 143.32, 149.85, 153.63, 160.75, 171.55; GC–MS: 313 $[M]^+$.

**1-((6-chloro-2-oxo-2H-chromen-4-yl)methyl)-4,4-dimethylpiperidine-2,6-dione (1c) [$C_{17}H_{16}ClNO_4$].** 4-(bromomethyl)-6-chloro-2H-chromen-2-one **(c)**: 2.73 g, 10 mM; Yield: 2.78 g (83.48%), yellow crystal; mp 312–313 °C; Anal. calcd. for. $C_{17}H_{16}ClNO_4$: C, 61.18; H, 4.83; N, 4.20. Found: C, 61.16; H, 4.85; N, 4.18; ATR-IR ($\nu_{max}$/cm$^{-1}$): 1725 (C═O of lactone), 1681(Cyclic C═O);$^{1}$H NMR (400 MHz, $CDCl_3$, $\delta$ ppm) 1.15 (s, 6H, –$CH_3$), 2.63 (s, 4H, –$CH_2$), 5.07 (s, 2H, –$CH_2$), 5.98 (s, 1H, –CH), 7.24–7.29 (m, 1H, Ar-H), 7.47–7.50(m, 1H, Ar-H) 7.63(d, 1H, $J$ = 2.4 Hz); $^{13}$C NMR (100 MHz, $CDCl_3$, δ ppm): 27.91, 29.31, 38.80, 46.10, 113.06, 118.68, 118.93, 123.43, 129.87, 131.97, 148.82, 151.96, 159.68, 171.48; GC–MS: 333$[M]^+$.

**1-((7-chloro-2-oxo-2H-chromen-4-yl)methyl)-4,4-dimethylpiperidine-2,6-dione (1d) [$C_{17}H_{16}ClNO_4$].** 4-(bromomethyl)-7-chloro-2H-chromen-2-one **(d)**: 2.73 g, 10 mM; Yield: 2.69 g (80.78%), yellow crystal; mp 318 – 319 °C; Anal. calcd. for. $C_{17}H_{16}ClNO_4$: C, 61.18; H, 4.83; N, 4.20. Found: C, 61.19; H, 4.86; N, 4.22; ATR-IR ($\nu_{max}$/cm$^{-1}$): 1721 (C═O of lactone), 1673 (Cyclic C═O); $^{1}$H NMR (400 MHz, $CDCl_3$, $\delta$ ppm) 1.12 (s, 6H, –$CH_3$), 2.62 (s, 4H, –$CH_2$), 5.06 (s, 2H, –$CH_2$), 5.96 (s, 1H, –CH), 7.24–7.32 (m, 2H, Ar-H), 7.58(d, 1H, $J$ = 8.8 Hz); $^{13}$C NMR (100 MHz, $CDCl_3$, δ ppm): 23.13, 23.20, 24.56, 34.11, 41.30, 107.37, 111.72, 112.76, 119.92, 120.16, 133.21, 144.55, 149.11, 154.85, 166.85; GC–MS: 333$[M]^+$.

**1-((5,7-dimethyl-2-oxo-2H-chromen-4-yl)methyl)-4,4-dimethylpiperidine-2,6-dione (1e) [$C_{19}H_{21}NO_4$].** 4-(bromomethyl)-5,7-dimethyl-2H-chromen-2-one**(e)**: 2.67 g, 10 mM; Yield: 2.51 g (76.75%), colourless crystal; mp 321–323 °C; Anal. calcd. for. $C_{19}H_{21}NO_4$: C, 69.71; H, 6.47; N, 4.28. Found: C, 69.73; H, 6.46; N, 4.26; ATR-IR ($\nu_{max}$/cm$^{-1}$): 1709 (C═O of lactone), 1670 (Cyclic C═O); $^{1}$H NMR (400 MHz , $CDCl_3$, $\delta$ ppm) 1.15 (s, 6H, –$CH_3$), 2.35 (s, 3H, –$CH_3$), 2.63 (s, 4H, –$CH_2$), 2.69 (s, 3H, –$CH_3$), 5.23 (s, 2H, –$CH_2$), 5.71 (s, 1H, –CH), 6.89 (s, 1H, Ar-H), 6.99(s, 1H, Ar-H); $^{13}$C NMR (100 MHz, $CDCl_3$, $\delta$ ppm): 21.15, 24.95, 28.03, 29.36, 42.54, 46.08, 109.64, 115.28, 116.29, 130.01, 135.47, 142.33, 152.06, 155.14, 160.48, 171.52; GC–MS: 327 $[M]^+$.

**1-((7,8-dimethyl-2-oxo-2H-chromen-4-yl)methyl)-4,4-dimethylpiperidine-2,6-dione (1f) [$C_{19}H_{21}NO_4$].** 4-(bromomethyl)-7,8-dimethyl-2H-chromen-2-one **(f)**: 2.67 g, 10 mM;Yield: 2.43 g (74.31%), colourless crystal; mp 308–309 °C; Anal. calcd. for. $C_{19}H_{21}NO_4$: C, 69.71; H, 6.47; N, 4.28. Found: C, 69.69; H, 6.48; N, 4.30; ATR-IR ($\nu_{max}$/cm$^{-1}$): 1721 (C═O of lactone), 1664 (Cyclic C═O); $^{1}$H NMR (400 MHz , $CDCl_3$, $\delta$ ppm) 1.13 (s, 6H, –$CH_3$), 2.32(s, 3H, –$CH_3$), 2.35 (s, 3H, –$CH_3$), 2.61 (s, 4H, –$CH_2$), 5.09 (s, 2H, –$CH_2$), 5.85 (s, 1H, –CH), 7.08 (d, 1H, $J$ = 8.4 Hz), 7.36(d, 1H, $J$ = 8.4 Hz) ; $^{13}$C NMR (100 MHz, $CDCl_3$, $\delta$ ppm): 11.64, 20.37, 27.97, 29.31, 39.11, 46.10, 110.03, 115.47, 120.26, 124.98, 125.76, 141.86, 150.29, 151.67, 161.03, 171.60; GC–MS: 327 $[M]^+$.

**1-((7-methoxy-2-oxo-2H-chromen-4-yl)methyl)-4,4-dimethylpiperidine-2,6-dione (1 g) [$C_{18}H_{19}NO_5$].** 4-(bromomethyl)-7-methoxy-2H-chromen-2-one**(g)**: 2.69 g, 10 mM; Yield: 2.71 g (82.37%), white solid; mp 273–275 °C ; Anal. calcd. for. $C_{18}H_{19}NO_5$: C, 65.64; H, 5.81; N, 4.25. Found: C, 65.62; H, 5.79; N, 4.24; ATR-IR ($\nu_{max}$/cm$^{-1}$): 1703 (C═O of lactone), 1669 (Cyclic C═O); $^{1}$H NMR (400 MHz , $CDCl_3$, $\delta$ ppm) 1.14 (s, 6H, –$CH_3$), 2.63 (s, 3H, –$OCH_3$), 3.85 (s, 4H, –$CH_2$), 5.08 (s, 2H, –$CH_2$), 5.80 (s, 1H, –CH), 6.81–6.87 (m, 2H, Ar-H), 7.55 (d, 1H, $J$ = 8.4 Hz); $^{13}$C NMR (100 MHz, $CDCl_3$, $\delta$ ppm): 27.94, 29.30, 38.97, 46.14, 55.76, 101.10, 108.66, 111.35, 112.55, 124.63, 150.03, 155.43, 160.97, 162.84, 171.60; GC–MS: 329 $[M]^+$.

**1-((6-bromo-2-oxo-2H-chromen-4-yl)methyl)-4,4-dimethylpiperidine-2,6-dione (1 h) [$C_{17}H_{16}BrNO_4$].** 6-bromo-4-(bromomethyl)–2H-chromen-2-one**(h)**: 3.17 g, 10 mM; Yield: 2.81 g (74.33%), light brown crystal; mp 324–325 °C; Anal. calcd. for. $C_{17}H_{16}BrNO_4$: C, 53.99; H, 4.26; N, 3.70. Found: C, 53.98; H, 4.24; N, 3.68; ATR-IR ($\nu_{max}$/cm$^{-1}$): 1715 (C═O of lactone), 1666 (Cyclic C═O); $^{1}$H NMR (400 MHz , $CDCl_3$, $\delta$ ppm) 1.15 (s, 6H, –$CH_3$), 2.63 (s, 4H, –$CH_2$), 5.07 (s, 2H, –$CH_2$), 5.96 (s, 1H, –CH), 7.21 (d, 1H, $J$ = 8.8 Hz), 7.61–7.63(m, 1H, Ar-H), 7.78(s, 1H, Ar-H); $^{13}$C NMR (100 MHz, $CDCl_3$, $\delta$ ppm): 27.94, 29.36, 38.86, 46.06, 112.82, 117.23, 119.01, 119.39, 126.45, 134.84, 148.78, 152.38, 159.70, 171.56; GC–MS: 378 $[M]^+$.

4,4-dimethyl-1-((3-oxo-3H-benzo[*f*]chromen-1-yl)methyl)piperidine-2,6-dione (1i)

**[$C_{21}H_{19}NO_4$].** 1-(bromomethyl)–3H-benzo[*f*]chromen-3-one **(i)**: 2.89 g, 10 mM; Yield: 2.91 g (76.98%), brown crystal; mp 343–344 °C; Anal. calcd. for. $C_{21}H_{19}NO_4$: C, 72.19; H, 5.48; N, 4.01. Found: C, 72.17; H, 5.50; N, 4.02; ATR-IR ($\nu_{max}$/cm$^{-1}$): 1713 (C═O of lactone), 1668 (Cyclic C═O); $^{1}$H NMR (400 MHz , $CDCl_3$, $\delta$ ppm) 1.16 (s, 6H, –$CH_3$), 2.65 (s, 4H, –$CH_2$), 5.56 (s, 2H, –$CH_2$), 5.97 (s, 1H, –CH), 7.40–7.62 (m, 3H, Ar-H), 7.88–7.96(m, 2H, Ar-H), 8.27(d, 1H, $J$ = 8.4 Hz); $^{13}$C NMR (100 MHz, $CDCl_3$, $\delta$ ppm): 28.03, 29.42, 43.50, 46.08, 110.41, 113.29, 117.70, 125.28, 125.60, 128.13, 129.36, 129.92, 131.41, 134.11, 152.59, 154.67, 160.30, 171.59; GC–MS: 378 $[M]^+$.

**4,4-dimethyl-1-((2-oxo-2H-benzo [*h*] chromen-4-yl)methyl)piperidine-2,6-dione (1j) [$C_{21}H_{19}NO_4$].** 4-(bromomethyl)–2H-benzo[*h*]chromen-2-one **(j)**: 2.89 g, 10 mM; Yield: 2.81 g (74.33%), pale yellow solid; mp 337 – 339 °C; Anal. calcd. for. $C_{21}H_{19}NO_4$: C, 72.19; H, 5.48;

N, 4.01. Found: C, 72.21; H, 5.49; N, 4.02; ATR-IR ($\nu_{max}/cm^{-1}$): 1719 (C=O of lactone), 1672 (Cyclic C=O); $^1$H NMR (400 MHz , $CDCl_3$, $\delta$ ppm) 1.17 (s, 6H, $-CH_3$), 2.65 (s, 4H, $-CH_2$), 5.23 (s, 2H, $-CH_2$), 6.03 (s, 1H, –CH), 7.61–7.72 (m, 4H, Ar-H), 7.84–7.87(m, 1H, Ar-H), 8.51–8.53(m, 1H, Ar-H); $^{13}$C NMR (100 MHz, $CDCl_3$, $\delta$ ppm): 28.00, 29.37, 39.48, 46.14, 110.89, 113.13, 119.12, 122.67, 123.14, 124.46, 127.31, 127.66, 128.89, 134.76, 150.85, 160.64, 171.62; GC–MS: 378 $[M]^+$.

### 3.4. Biological assay

#### 3.4.1. Antidiabetic activity

Antidiabetic activity was assessed using 2-NBDG uptake assay. Insulin resistance HepG2 (human liver carcinoma) cells were seeded in 96 well plate with 70% confluency and further treated with a mixture of fructose, palmitic acid, TNF-alpha, Metformin and test compounds. After 24 h incubation, the cells were washed with 40 μM 2-NBDG and PBS (1 X). Simultaneously, for every hour 100 nM insulin were added in each of the wells. The cells were carefully washed again and later lysis buffer was added, after which the fluorescence reading were taken from each well.

Control refers to cells cultured only in DMEM + 10%FBS + 1% antibiotic for 24 h prior to the 2-NBDG uptake analysis. TEST refers to the cells which were grown in insulin resistance media for 24 h prior to 2-NBDG uptake analysis. Insulin resistance media consists of DMEM + 10% FBS + 1% antibiotic along with combination of 20 ng/mL TNF-alpha, 0.1 mM of palmitic acid and 40 mM of fructose. This mixture was used basically to induce insulin resistance in the HepG2 cell line. Different doses of different compounds were given to the cells along with insulin resistance media for 24 h prior to the 2-NBDG uptake.

#### 3.4.2. Cytotoxicity assay

HEK-293 cells (human embryonic kidney cells) were grown in Dulbecco's modified eagle's medium supplemented with 10% fasting blood sugar and 1% of antibiotic at 37 °C under 5% of carbon dioxide. Cells were later harvested using trypsin and seeded in a 96-well cell culture plate for the MTT (3-(4,5-Dimethylthiazol-2-yl)-2,5-diphenyltetrazolium bromide) assay. The test compounds were solubilised in cell culture grade DMSO. Once the cells in 96-well plate were 70% confluent, the compounds were injected to the cells at 50 nM to 10000 nM concentration (made in DMEM supplemented with 1% antibiotic and 10% FBS) for 24 h. After 24 h, cells were washed with PBS and added with 100 μL of fresh media in each well along with 10 μL of MTT reagent (5 mg/mL) for another 4 h. After 4 h, media was again removed and added 100 μL cell culture grade DMSO to dissolve the formazan crystals formed by the reduction of MTT by the live cells. Absorbance of the solution were taken at 570 nm.

### 3.5. pH titrimetric assay

In water and acetonitrile mixture (8:2) [55], stock solutions for KOH (25 mM), HCl (25 mM) and test compounds (0.5 mM) were prepared. Potentiometric titration method was employed to determine the $pK_a$ values of compounds. UV–Visible Spectrophotometer was used to study the absorbance spectra of the test compounds.

### 3.6. HSA interaction study using spectroscopic and in-silico methods

Standard stock solution of the most active antidiabetic compound **1f** (1 mM) was prepared by dissolution in DMSO. A standard solution of HSA (5 μM) was prepared in pH 7.4 sodium phosphate buffer and this solution was incubated for 24 h. The absorbance of this solution was measured at 280 nm to accurately calculate the concentration of HSA standard solution by knowing the molar absorption coefficient of HSA ($\varepsilon$ = 36,500 $M^{-1}cm^{-1}$) [41]. For the titration studies, HSA absorbance spectra were recorded on a UV–Visible Spectrophotometer (1800 SHIMADZU) using cuvettes of 1.0 cm path length. HSA fluorescence emission spectra were recorded using a 150 W xenon lamp equipped RF-5301pc SHIMADZU Spectrofluorophotometer.

All the fluorescence emission intensities were corrected with the absorbance of compound **1f** to eliminate inner filter effects [42,53]. Eq. (8) was used for this correction.

$$F_{corr} = F_{obsd}\, 10^{(A_1+A_2)/2} \quad (8)$$

where $F_{corr}$ and $F_{obsd}$ are the corrected and observed emission intensities of **1f**, respectively; $A_1$ and $A_2$ are sum of absorbances of **1f** and HSA at the emission and excitation wavelengths, respectively.

Molecular docking studies were performed to determine the potential binding environment between HSA and **1f**. The structure of HSA (PDB ID: 1AO6) was acquired from the Protein Data Bank. The 3D structure of **1f** was produced by 3D ChemDraw Ultra 8.0 and MM2 force-field was applied for energy minimization. Docking studies were carried using the molecular docking software (AutoDock4.2). AutoDock Tools (ADTs) produce various ligand conformers using a Lamarckian genetic algorithm (LGA) which is built on adaptive local method search. Docking was carried out by setting the grid size to 60, 50, 80 along x, y, z axes with a grid spacing 0.375 Å. The grid centre was set as 22.556, 35.519, 97.262 Å. The grid map for different atoms of **1f** and HSA was generated by running the AutoGrid. Upon generation of grid maps, AutoDock was ran and Autodock parameters were found to be as follows: GA population size: 150; Numbers of generations: 27000; Maximum numbers of energy evaluations: $2.5 \times 10^6$ [53]. A total of 10 runs were performed, and out of all those, minimum energy conformers were picked for the study based on ranking and scoring.

## 4. Conclusions

In the present study, we describe the design, synthesis and evaluation of coumarin-cyclic imides **(1a–1j)** as possible antidiabetic agents. Among synthesized, compound **1f** exhibited distinct activity with 85.21% of glucose uptake which is comparable with standard drug Metformin (93.25% glucose uptake). All the compounds **(1a–1j)** were observed to be least toxic against Human Embryonic Kidney cells indicating their good safety profile. Single crystals of compounds **1a**, **1b**, **1c**, **1d**, **1e**, **1f**, **1h** and **1i** were developed and their crystal parameters were evaluated. A notable observation from X-ray crystal studies was that compounds **1f** and **1b** which exhibited significant glucose uptake activity have shown C=O-π interactions in X-ray crystal packing. The solution stability studies indicated that the test compounds are sufficiently stable at varied pH conditions and thereby compatible with biophysiological environments. HSA interaction studies using spectroscopic methods showed that compound **1f** binds to HSA through favourable and facile binding reaction and thereby can be used for *in-vivo* testing. Molecular docking results suggest that the main force involved in binding of **1f** with HSA is hydrophobic interaction, whereas hydrogen bonds might have a minor contribution in the interaction between **1f** and HSA. The results obtained clearly indicates that compound **1f** can act as a promising lead for developing new class of possible antidiabetic drugs and may shed light in exploring newer coumarin-cyclic imide derivatives towards diabetic research and development.

## Declaration of Competing Interest

The authors declare no conflict of interest.

## Acknowledgements

Amit Kumar is grateful to SERB, Department of Science and Technology for research grant (SB/FT/CS-100/2013), and Centre for Nano and Material Sciences, Jain University, Bangalore, India for

providing infrastructural facilities and financial support.

## Appendix A. Supplementary material

Single crystal X-ray data for compounds **1a, 1b, 1c, 1d, 1e, 1f, 1h** and **1i** have been deposited with the Cambridge Crystallographic Data Centre with CCDC No. 1850002, 1850003, 1850004, 1850005, 1850006, 1850007, 1850008 and 1850009 respectively. $^{1}H$ and $^{13}C$ NMR spectrum of all the new compounds, pH titration curves and UV-Visible spectra of tested compounds, selected bond lengths [Å] & bond angles [°], structural correlation between X-ray crystal structure and antidiabetic activity are given in supporting Information. Supplementary data to this article can be found online at https://doi.org/10.1016/j.bioorg.2019.103212.

## References


[1] WHO report, Global report on diabetes, 2016.
[2] Y. Lin, Z. Sun, Current views on type 2 diabetes, J. Endocrinol. 204 (2010) 1.
[3] A. Chaudhury, C. Duvoor, R. Dendi, V. Sena, S. Kraleti, A. Chada, R. Ravilla, A. Marco, N.S. Shekhawat, M.T. Montales, Clinical review of antidiabetic drugs: Implications for type 2 diabetes mellitus management, Front. Endocrinol. 8 (2017) 6.
[4] B.D. Green, P.R. Flatt, C.J. Bailey, Dipeptidyl peptidase IV (DPP IV) inhibitors: a newly emerging drug class for the treatment of type 2 diabetes, Diabetes Vasc. Dis. Res. 3 (3) (2006) 159–165.
[5] T. Biftu, R. Sinha-Roy, P. Chen, X. Qian, D. Feng, J.T. Kuethe, G. Scapin, Y.D. Gao, Y. Yan, D. Krueger, A. Bak, G. Eiermann, J. He, J. Cox, J. Hicks, K. Lyons, H. He, G. Salituro, S. Tong, S. Patel, G. Doss, A. Petrov, J. Wu, S.S. Xu, C. Sewall, X. Zhang, B. Zhang, N.A. Thornberry, A.E. Weber, Omarigliptin (MK-3102): a novel long-acting DPP-4 inhibitor for once-weekly treatment of type 2 diabetes, J. Med. Chem. 57 (2014) 3205–3212.
[6] S. Bolen, L. Feldman, J. Vassy, L. Wilson, H.-C. Yeh, S. Marinopoulos, C. Wiley, E. Selvin, R. Wilson, E.B. Bass, Systematic review: comparative effectiveness and safety of oral medications for type 2 diabetes mellitus, Ann. Intern. Med. 147 (6) (2007) 386–399.
[7] F. Salvo, N. Moore, M. Arnaud, P. Robinson, E. Raschi, F. De Ponti, B. Bégaud, A. Pariente, Addition of dipeptidyl peptidase-4 inhibitors to sulphonylureas and risk of hypoglycaemia: systematic review and meta-analysis, BMJ 353 (2016) i2231.
[8] T. Karagiannis, E. Bekiari, P. Boura, A. Tsapas, Cardiovascular risk with DPP-4 inhibitors: latest evidence and clinical implications, Ther. Adv. Drug. Saf. 7 (2016) 36–38.
[9] (a) G. Keating, R. O'kennedy, The Chemistry and Occurrence of Coumarins, Coumarins: Biology, Applications and Mode of Action, John Wiley & Sons Inc, New York, NY, 1997, p. 348;
(b) D.S. Reddy, K.M. Hosamani, H.C. Devarajegowda, M.M. Kurjogi, A facile synthesis and evaluation of new biomolecule-based coumarin–thiazoline hybrids as potent anti-tubercular agents with cytotoxicity, DNA cleavage and X-ray studies, RSC Adv. 5 (79) (2015) 64566–64581.
[10] (a) C. Kontogiorgis, A. Detsi, D. Hadjipavlou-Litina, Coumarin-based drugs: a patent review (2008–present), Expert Opin. Ther. Pat. 22 (4) (2012) 437–454;
(b) K.M. Hosamani, D.S. Reddy, H.C. Devarajegowda, Microwave-assisted synthesis of new fluorinated coumarin–pyrimidine hybrids as potent anticancer agents, their DNA cleavage and X-ray crystal studies, RSC Adv. 5 (15) (2015) 11261–11271.
[11] D.S. Reddy, K.M. Hosamani, H.C. Devarajegowda, Design, synthesis of benzocoumarin-pyrimidine hybrids as novel class of antitubercular agents, their DNA cleavage and X-ray studies, Eur. J. Med. Chem. 101 (2015) 705–715.
[12] R.N. Chopra, 1882-. Chopra's indigenous drugs of India. 2nd ed., rev. and largely rewritten Calcutta : U.N. Dhur and Sons xxxii (1958) 816.
[13] P. Seema, B. Sudha, P. Pius, S.A. Asha, K. Raghu, C. Paulose, Kinetic studies of purified malate dehydrogenase in liver of streptozotocindiabetic rats and the effect of leaf extract of Aegle marmelose (L.) Correa ex Roxb, Indian J. Exp. Biol. 34 (1996) 600–602.
[14] P. Ponnachan, C. Paulose, K. Panikkar, Effect of leaf extract of Aegle marmelose in diabetic rats, Indian J. Exp. Biol 31 (1993) 345–347.
[15] (a) H. Li, Y. Yao, L. Li, Coumarins as potential antidiabetic agents, J. Pharm. Pharmacol. 69 (10) (2017) 1253–1264;
(b) D. Prabakaran, N. Ashokkumar, Protective effect of esculetin on hyperglycemia-mediated oxidative damage in the hepatic and renal tissues of experimental diabetic rats, Biochimie 95 (2) (2013) 366–373;
(c) S.-J. Wu, Osthole attenuates inflammatory responses and regulates the expression of inflammatory mediators in HepG2 cells grown in differentiated medium from 3T3-L1 preadipocytes, J. Med. Food 18 (9) (2015) 972–979;
(d) K.S. Kang, W. Lee, Y. Jung, J.H. Lee, S. Lee, D.-W. Eom, Y. Jeon, H.H. Yoo, M.J. Jin, K.I. Song, Protective effect of esculin on streptozotocin-induced diabetic renal damage in mice, J. Agric. Food. Chem. 62 (9) (2014) 2069–2076;
(e) M.N. Islam, H.A. Jung, H.S. Sohn, H.M. Kim, J.S. Choi, Potent α-glucosidase and protein tyrosine phosphatase 1B inhibitors from Artemisia capillaris, Arch. Pharmacal Res. 36 (5) (2013) 542–552;
(f) A.J. Scheen, Is there a role for α-glucosidase inhibitors in the prevention of type 2 diabetes mellitus? Drugs 63 (10) (2003) 933–951.
[16] W.-H. Lee, H.-H. Wu, W.-J. Huang, Y.-N. Li, R.-J. Lin, S.-Y. Lin, Y.-C. Liang, N-hydroxycinnamide derivatives of osthole ameliorate hyperglycemia through activation of AMPK and p38 MAPK, Molecules 20 (3) (2015) 4516–4529.
[17] C. Sun, C. Peng, J. Wang, Q. Wang, W. Liu, H. Zhou, C. Yang, Synthesis of novel coumarin derivatives and in vitro biological evaluation as potential PTP 1B inhibitors, Heterocycles 87 (2013) 1711–1726.
[18] J. Han, L. Sun, X. Huang, Z. Li, C. Zhang, H. Qian, W. Huang, Novel coumarin modified GLP-1 derivatives with enhanced plasma stability and prolonged in vivo glucose-lowering ability, Br. J. Pharmacol. 171 (23) (2014) 5252–5264.
[19] M.K. Hargreaves, J. Pritchard, H. Dave, Cyclic carboxylic monoimides, Chem. Rev. 70 (4) (1970) 439–469.
[20] S.R.T. Prado, V. Cechinel-Filho, F.C. Buzzi, R. Corrêa, S.M.C.S. Cadena, M.B.M. de Oliveira, Biological evaluation of some selected cyclic imides: Mitochondrial effects and in vitro cytotoxicity, Zeitschrift für Naturforschung C 59 (9–10) (2004) 663–672.
[21] B.S. Kim, S.S. Moon, B.K. Hwang, Isolation, Antifungal Activity, and Structure Elucidation of the Glutarimide Antibiotic, Streptimidone, Produced by Micromonospora c oerulea, J. Agric. Food. Chem. 47 (8) (1999) 3372–3380.
[22] A. Kumar, N. Kumar, P. Roy, S. Sondhi, A. Sharma, Synthesis of acridine cyclic imide hybrid molecules and their evaluation for anticancer activity, Med. Chem. Res. 24 (8) (2015) 3272–3282.
[23] K.N. de Oliveira, L.D. Chiaradia, P.G.A. Martins, A. Mascarello, M.N.S. Cordeiro, R.V.C. Guido, A.D. Andricopulo, R.A. Yunes, R.J. Nunes, J. Vernal, Sulfonyl-hydrazones of cyclic imides derivatives as potent inhibitors of the Mycobacterium tuberculosis protein tyrosine phosphatase B (PtpB), MedChemComm 2 (6) (2011) 500–504.
[24] W.G. Maurice, 4,4-dimethylpiperidine-2,6-dione derivatives for use in the treatment of hypertension, Patent no. WO 2007031737 A1, Prestwick Pharmaceuticals, Inc.
[25] K. Kaku, First novel once-weekly DPP-4 inhibitor, trelagliptin, for the treatment of type 2 diabetes mellitus, Expert Opin. Pharmacother. 16 (16) (2015) 2539–2547.
[26] J. Feng, Z. Zhang, M.B. Wallace, J.A. Stafford, S.W. Kaldor, D.B. Kassel, M. Navre, L. Shi, R.J. Skene, T. Asakawa, Discovery of alogliptin: a potent, selective, bioavailable, and efficacious inhibitor of dipeptidyl peptidase IV, J. Med. Chem. 50 (10) (2007) 2297–2300.
[27] A.H. Barnett, H. Huisman, R. Jones, M. von Eynatten, S. Patel, H.-J. Woerle, Linagliptin for patients aged 70 years or older with type 2 diabetes inadequately controlled with common antidiabetes treatments: a randomised, double-blind, placebo-controlled trial, The Lancet 382 (9902) (2013) 1413–1423.
[28] O. El-Kabbani, C. Darmanin, M. Oka, C. Schulze-Briese, T. Tomizaki, I. Hazemann, A. Mitschler, A. Podjarny, High-resolution structures of human aldose reductase holoenzyme in complex with stereoisomers of the potent inhibitor Fidarestat: stereospecific interaction between the enzyme and a cyclic imide type inhibitor, J. Med. Chem. 47 (18) (2004) 4530–4537.
[29] P.J. Oates, B.L. Mylari, Aldose reductase inhibitors: therapeutic implications for diabetic complications, Expert Opin. Invest. Drugs 8 (12) (1999) 2095–2119.
[30] M.A. Pfeifer, M.P. Schumer, D.A. Gelber, Aldose reductase inhibitors: the end of an era or the need for different trial designs? Diabetes 46 (Supplement 2) (1997) S82–S89.
[31] A.-M. Alaa, A.S. El-Azab, S.M. Attia, A.M. Al-Obaid, M.A. Al-Omar, H.I. El-Subbagh, Synthesis and biological evaluation of some novel cyclic-imides as hypoglycaemic, anti-hyperlipidemic agents, Eur. J. Med. Chem. 46 (9) (2011) 4324–4329.
[32] C.A. Lipinski, F. Lombardo, B.W. Dominy, P.J. Feeney, Experimental and computational approaches to estimate solubility and permeability in drug discovery and development settings, Adv. Drug Deliv. Rev. 23 (1–3) (1997) 3–25.
[33] P.D. Leeson, B. Springthorpe, The influence of drug-like concepts on decision-making in medicinal chemistry, Nat. Rev. Drug Discovery 6 (11) (2007) 881.
[34] M.V. Kulkarni, B.G. Pujar, V.D. Patil, Studies on coumarins, II6, Arch. Pharm. 316 (1) (1983) 15–21.
[35] G.M. Sheldrick, Crystal structure refinement with SHELXL, Acta Crystallographica Section C: Struct. Chem. 71 (1) (2015) 3–8.
[36] G.M. Sheldrick, Acta Crystallogr. Sect. C: Struct. Chem. 71 (2015) 3–8.
[37] (a) D.S. Reddy, M. Kongot, S.P. Netalkar, M.M. Kurjogi, R. Kumar, F. Avecilla, A. Kumar, Synthesis and evaluation of novel coumarin-oxime ethers as potential anti-tubercular agents: their DNA cleavage ability and BSA interaction study, Eur. J. Med. Chem. 150 (2018) 864–875;
(b) S. Babić, A.J. Horvat, D.M. Pavlović, M. Kaštelan-Macan, Determination of pKa values of active pharmaceutical ingredients, TrAC, Trends Anal. Chem. 26 (11) (2007) 1043–1061.
[38] (a) H. Fischer, R. Gottschlich, A. Seelig, Blood-brain barrier permeation: molecular parameters governing passive diffusion, J. Membr. Biol. 165(3) (1998) 201-211; (b) M. Kongot, N. Dohare, V. Singh, D. Reddy, N.K. Singhal, R. Patel, A. Kumar, A novel biocompatible NiII tethered moiety as a glucose uptake agent and a hit against methicillin-resistant Staphylococcus aureus, Eur. J. Pharm. Sci. 123 (2018) 335–349; (c) M. Kongot, D. Reddy, V. Singh, R. Patel, N.K. Singhal, A. Kumar, Potent drug candidature of an ONS donor tethered copper (II) complex: Anticancer activity, cytotoxicity and spectroscopically approached BSA binding studies, Spectrochim. Acta Part A: Mol. Biomol. Spectrosc. 212 (2019) 330–342.
[39] (a) T.A. Wani, A.H. Bakheit, S. Zargar, M.A. Bhat, A.A. Al-Majed, Molecular docking and experimental investigation of new indole derivative cyclooxygenase inhibitor to probe its binding mechanism with bovine serum albumin, Bioorg. Chem. 89 (2019) 103010;
(b) M. Kongot, N. Dohare, D.S. Reddy, N. Pereira, R. Patel, M. Subramanian, A. Kumar, In vitro apoptosis-induction, antiproliferative and BSA binding studies of a oxidovanadium (V) complex, J. Trace Elem. Med Biol. 51 (2019) 176–190;

(c) M. Kongot, D. Reddy, V. Singh, R. Patel, N.K. Singhal, A. Kumar, ONS donor entwined iron(III) and cobalt(III) complexes with exemplary safety profile as potent anticancer and glucose uptake agents, New J. Chem. 43 (2019) 10932–10947;
(d) M. Kongot, N. Maurya, N. Dohare, M. Parray, J. Kumar, A. Kumar, R. Patel, Enthalpy-driven interaction between dihydropyrimidine compound and bovine serum albumin: A spectroscopic and computational approach, J. Biomol. Struct. Dyn. 36 (2018) 1161–1170.

[40] G. Colmenarejo, In silico prediction of drug-binding strengths to human serum albumin, Med. Res. Rev. 23 (3) (2003) 275–301.

[41] M. Kumari, J.K. Maurya, M. Tasleem, P. Singh, R. Patel, Probing HSA-ionic liquid interactions by spectroscopic and molecular docking methods, J. Photochem. Photobiol., B 138 (2014) 27–35.

[42] (a) J.R. Lakowicz, Principles of Fluorescence Spectroscopy, third ed., Springer, New York, 2006, p. 268;
(b) S. Bi, L. Yan, Y. Sun, H. Zhang, Investigation of ketoprofen binding to human serum albumin by spectral methods, Spectrochim. Acta Part A Mol. Biomol. Spectrosc. 78 (1) (2011) 410–414.

[43] (a) J.K. Maurya, A.B. Khan, N. Dohare, A. Ali, A. Kumar, R. Patel, Effect of aromatic amino acids on the surface properties of 1-dodecyl-3-(4-(3-dodecylimidazolidin-1-yl) butyl) imidazolidine bromide gemini surfactant, J. Dispersion Sci. Technol. 39 (2) (2018) 174–180;
(b) P.D. Ross, S. Subramanian, Thermodynamics of protein association reactions: forces contributing to stability, Biochemistry 20 (11) (1981) 3096–3102.

[44] F. Samari, B. Hemmateenejad, M. Shamsipur, M. Rashidi, H. Samouei, Affinity of two novel five-coordinated anticancer Pt (II) complexes to human and bovine serum albumins: a spectroscopic approach, Inorg. Chem. 51 (6) (2012) 3454–3464.

[45] P. Kalaivani, R. Prabhakaran, E. Vaishnavi, T. Rueffer, H. Lang, P. Poornima, R. Renganathan, V.V. Padma, K. Natarajan, Synthesis, structure, DNA/protein binding and in vitro cytotoxicity of new ruthenium metallates, Inorg. Chem. Frontiers 1 (4) (2014) 311–324.

[46] C. Jash, P.V. Payghan, N. Ghoshal, G. Suresh Kumar, Binding of the iminium and alkanolamine forms of sanguinarine to lysozyme: spectroscopic analysis, thermodynamics, and molecular modeling studies, J. Phys. Chem. B 118 (46) (2014) 13077–13091.

[47] X. Pan, R. Liu, P. Qin, L. Wang, X. Zhao, Spectroscopic studies on the interaction of acid yellow with bovine serum albumin, J. Lumin. 130 (4) (2010) 611–617.

[48] C. Jash, G.S. Kumar, Binding of alkaloids berberine, palmatine and coralyne to lysozyme: a combined structural and thermodynamic study, RSC Adv. 4 (24) (2014) 12514–12525.

[49] D. Beljonne, C. Curutchet, G.D. Scholes, R.J. Silbey, Beyond Forster resonance energy transfer in biological and nanoscale systems, J. Phys. Chem. B 113 (19) (2009) 6583–6599.

[50] F.-L. Cui, J. Fan, D.-L. Ma, M.-C. Liu, X.-G. Chen, Z.-D. Hu, A study of the interaction between a new reagent and serum albumin by fluorescence spectroscopy, Anal. Lett. 36 (10) (2003) 2151–2166.

[51] M. Asadi, Z. Asadi, S.B. Sadi, L. Zarei, F.M. Baigi, Z. Amirghofran, Synthesis, characterization and the interaction of some new water-soluble metal Schiff base complexes with human serum albumin, Spectrochim. Acta Part A Mol. Biomol. Spectrosc. 122 (2014) 118–129.

[52] X.-X. Cheng, Y. Lui, B. Zhou, X.-H. Xiao, Y. Liu, Probing the binding sites and the effect of berbamine on the structure of bovine serum albumin, Spectrochim. Acta Part A Mol. Biomol. Spectrosc. 72 (5) (2009) 922–928.

[53] N. Maurya, J.K. Maurya, U.K. Singh, R. Dohare, M. Zafaryab, M.M.A. Rizvi, M. Kumari, R. Patel, In vitro cytotoxicity and interaction of noscapine with human serum albumin: effect on structure and esterase activity of HSA, Mol. Pharm. 16 (3) (2019) 952–966.

[54] G. Rabbani, M.H. Baig, E.J. Lee, W.-K. Cho, J.Y. Ma, I. Choi, Biophysical study on the interaction between eperisone hydrochloride and human serum albumin using spectroscopic, calorimetric, and molecular docking analyses, Mol. Pharm. 14 (5) (2017) 1656–1665.

[55] J. Beltran, N. Sanli, G. Fonrodona, D. Barron, G. Özkan, J. Barbosa, Spectrophotometric, potentiometric and chromatographic pKa values of polyphenolic acids in water and acetonitrile–water media, Anal. Chim. Acta 484 (2) (2003) 253–264.